nature communications

Article

https://doi.org/10.1038/s41467-024-53290-6

Polyphenol-mediated redox-active hydrogel with H_2S gaseous-bioelectric coupling for periodontal bone healing in diabetes

Received: 31 August 2023

Accepted: 8 October 2024

Published online: 21 October 2024

Check for updates

Xinyi Fang[1,2,3,4,6], Jun Wang[2,6], Chengxinyue Ye[2], Jiu Lin[2,4], Jinhui Ran[3], Zhanrong Jia[3,5], Jinglei Gong[2], Yiming Zhang[3], Jie Xiang[2], Xiong Lu[3], Chaoming Xie[3] ✉ & Jin Liu[1] ✉

Excessive oxidative response, unbalanced immunomodulation, and impaired mesenchymal stem cell function in periodontitis in diabetes makes it a great challenge to achieve integrated periodontal tissue regeneration. Here, a polyphenol-mediated redox-active algin/gelatin hydrogel encapsulating a conductive poly(3,4-ethylenedioxythiopene)-assembled polydopamine-mediated silk microfiber network and a hydrogen sulfide sustained-release system utilizing bovine serum albumin nanoparticles is developed. This hydrogel is found to reverse the hyperglycemic inflammatory microenvironment and enhance functional tissue regeneration in diabetic periodontitis. Polydopamine confers the hydrogel with anti-oxidative and anti-inflammatory activity. The slow, sustained release of hydrogen sulfide from the bovine serum albumin nanoparticles recruits mesenchymal stem cells and promotes subsequent angiogenesis and osteogenesis. Moreover, poly(3,4-ethylenedioxythiopene)-assembled polydopamine-mediated silk microfiber confers the hydrogel with good conductivity, which enables it to transmit endogenous bioelectricity, promote cell arrangement, and increase the inflow of calcium ion. In addition, the synergistic effects of hydrogen sulfide gaseous-bioelectric coupling promotes bone formation by amplifying autophagy in periodontal ligament stem cells and modulating macrophage polarization via lipid metabolism regulation. This study provides innovative insights into the synergistic effects of conductivity, reactive oxygen species scavenging, and hydrogen sulfide on the periodontium in a hyperglycemic inflammatory microenvironment, offering a strategy for the design of gaseous-bioelectric biomaterials to promote functional tissue regeneration in immune-related diseases.

Periodontitis is an infection-driven inflammatory disease which can cause irreversible damage to the periodontal tissue and subsequently tooth loss[1,2]. The severity of periodontitis is increased by diabetes mellitus, even with little dental plaque accumulation[3]. Both the innate and adaptive immune systems, which contribute to periodontium damage, are affected by diabetes[3]. In addition, as periodontitis-derived inflammatory factors released into the bloodstream, glycemic control is adversely affected and the severity of diabetic complications could be increased[4,5]. Hence, the treatment of periodontitis in diabetes patient is important not only for the preservation of dentition, but also to minimize the effects of the periodontitis-induced systemic inflammatory burden on glycemic control and diabetic complications.

A full list of affiliations appears at the end of the paper. ✉e-mail: xie@swjtu.edu.cn; liujin@scu.edu.cn

Currently, general strategies for the treatment of periodontitis and alveolar bone regeneration include subgingival instrumentation accompanied by regenerative periodontal surgery as well as local administration of antibiotics and/or bioactive molecules[6–10]. However, the beneficial effects of these operations are limited by the over-activated oxidative stress response, excessive inflammation, unbalanced immunomodulation, and impaired mesenchymal stem cell (MSC) function present under diabetic conditions[11,12]. Insufficient new alveolar bone formation, secondary bone resorption, and recurrence of infection are frequently seen during the treatment of diabetic periodontitis[13]. Guided bone/tissue regeneration (GBR/GTR), such as collagen based matrix, pericardium membranes and functionally gradient membranes, are widely used to reconstruct alveolar bone in periodontitis. However, traditional GBR/GTR membranes are used as the physical barrier. Although recent GBR/GTR membranes have been endowed with biological properties to promote periodontal bone regeneration[14,15], the therapeutic effects of these membranes are limited by the diabetes-aggravated inflammatory environment.

Endogenous signaling such as bioelectric, mechanical and gaseous signalings mediate dramatic changes in the composition of cells, tissues and their microenvironments, and subsequently orchestrate the healing process[16–19]. In particular, hydrogen sulfide (H_2S), an endogenous gasotransmitter, influences several physiological and pathophysiological processes[20]. It is reported to alleviate alveolar bone resorption in periodontitis through attenuating inflammation, apoptosis, and reactive oxygen species (ROS)[21,22]. Moreover, the osteogenic function of H_2S in periodontal tissue has been established[23]. However, the biosynthesis of H_2S is impaired in diabetes patients, which has an adverse effect on MSC migration, angiogenesis, inflammation control and subsequently tissue regeneration[24–28]. Recently, although many efforts have attempted to produce exogenous H_2S in wounds using H_2S donors such as inorganic sulfide salt, GYY4137, and DTTs, their uncontrollably fast rate of H_2S generation and poor water solubility have limited their therapeutic effects and clinical applications[29,30].

Bioelectricity is an important physiological activity in the human body, mostly realized through endogenous electric fields such as membrane potential and nerve potential[17,31]. Endogenous electrical signals can modulate myriad biological processes, from the cell cycle, migration, proliferation and differentiation to nerve conduction, muscle contraction, embryogenesis and tissue regeneration[17,32–35]. Notably, electrical signals generated by mechanical stress act as stimuli for bone growth and remodeling[36]. Moreover, electrical signals improve cell arrangement, which is essential for functional periodontium regeneration[17,32,37]. Unfortunately, it is difficult for traditional GBR/GTR membranes to transmit endogenous electrical signals due to their lack of conductivity. Thus, functional and conductive GBR/GTR membranes to couple endogenous bioelectric signals have great potential for diabetic periodontal tissue regeneration[31].

Hydrogels have gained increasing attention in the field of periodontal tissue regeneration due to their structure and composition, which are similar to natural extracellular matrix[38,39]. In the diabetic periodontal environment, locally aggravated inflammatory responses can be attenuated by hydrogels with immunomodulatory ability to reverse the inflammatory conditions. However, most of these hydrogels have been designed with a focus on the delivery of growth factors or stem cells[38–40], with a lack of attention to the biological effects of the main components of the hydrogels. In addition, conductive hydrogel designs usually use conductive fillers such as ionic liquids, conductive polymers, carbon and metal nanoparticles. Biosafety concerns about the potential leakage of ionic liquid, the aggregation caused by the hydrophobicity of conductive polymers and nanoparticles, and the lack of biofunctionality have limited these conductive fillers used in the construction of conductive immunomodulatory hydrogels. Polyphenols such as tannic acid, pyrogallol, gallic acid and dopamine have been widely applied to functionalize hydrogels due to their abundant catechol and pyrogallol groups. Moreover, polyphenols also exhibit excellent biocompatibility, antioxidant properties, and immunomodulatory activity[41]. Our previous studies have demonstrated that polyphenol-mediated strategies can promote the hydrophilicity of conductive fillers, ensuring their uniform dispersion throughout hydrogel networks. At the same time, polyphenol-mediated conductive fillers endow these hydrogels with desirable biological functions such as transmitting bioelectrical signals to promote tissue regeneration.

In this study, we developed a polyphenol-mediated redox-active algin/gelatin (AG) hydrogel possessing a H_2S sustained-release system as well as a conductive poly(3,4-ethylenedioxythiopene)-assembled polydopamine-mediated silk microfiber (PEDOT-PSF) network to couple endogenous electrical and gaseous signals. The H_2S sustained-release system was constructed using NaHS-encapsulated bovine serum albumin nanoparticles (BNPs). The PEDOT-PSF networks were fabricated using a polyphenol-mediated protection-extraction strategy. The PEDOT-PSF uniformly distributed throughout the hydrogel, enhancing its mechanical and conductive properties. With its H_2S sustained-release and conductivity, the hydrogel can couple endogenous electrical and gaseous signals, promoting MSC recruitment, cell arrangement, angiogenesis and osteogenesis as well as M2 macrophage polarization. These properties enable the hydrogel to reverse the inflammatory microenvironment, creating a pro-regenerative microenvironment in a hyperglycemic inflammatory microenvironment (Fig. 1).

Results

Design strategies

To couple endogenous electrical signals, the conductive pathway in a hydrogel is essential. PEDOT-PSF was used to construct the conductive pathway in our AG hydrogel network. First, the PSF was extracted from raw silk via a polydopamine (PDA)-mediated protection-extraction process. After extraction, the catechol groups on the surface of the PSF serve as anchor sites to induce EDOT self-assembly in situ (Fig. 1a). To rescue downregulated H_2S levels in periodontitis in diabetic environment (Supplementary Fig. 1), NaHS was encapsulated in BNPs using a desolvation method to release H_2S persistently (Fig. 1b). To avoid NaHS exposure to water in the process of fabrication, NaHS was resolved in ethanol phase. AG hydrogel was crosslinked with Poly (ethylene glycol) diglycidyl ether (PEGDE) and Ca^{2+}, and enhanced by PEDOT-PSF (Fig. 1c). In the hydrogel matrix, the electron transfer from PEDOT to PDA induces the catechol-quinone redox balance of PDA, such that there remain abundant catechol groups for the hydrogel. The catechol-quinone redox balance plays an important role in scavenging ROS, relieving oxidative stress, and modulating local immune responses (Fig. 1d). Moreover, the conductive hydrogel couples endogenous electrical signals to ameliorate cell arrangement, increase Ca^{2+} internal flow, and subsequently potentiate osteogenesis (Fig. 1e). Meanwhile, the low concentration of H_2S released by BNPs replenishes the impaired endogenous gas signals to promote MSC recruitment, angiogenesis and osteogenesis as well as M2 macrophage polarization (Fig. 1f). Therefore, the catechol-quinone redox balance, electroactivity, and H_2S release of the hydrogel synergistically promote diabetic periodontal tissue regeneration.

Characterization of the hydrogel

The successful assembly of PDA and PEDOT on the surface of silk microfiber (mSF) was verified using scanning electron microscopy (SEM) (Fig. 2a–c). The cross-section image showed that after assembly of PEDOT on the surface of PSF, the surface of PEDOT-PSF is rougher than that of mSF and PSF (Supplementary Fig. 2a). The element mapping of the PEDOT-PSF showed the present of S element in the PEDOT-PSF, confirming the successful assembly of PEDOT on the surface of PSF (Fig. 2d). XRD and FTIR showed in Supplementary Fig. 2b, c also proved the successful assembly of PEDOT on mSF. The BNPs appeared spherical, with a diameter of approximately 300 nm (Fig. 2e).

https://doi.org/10.1038/s41467-024-53290-6

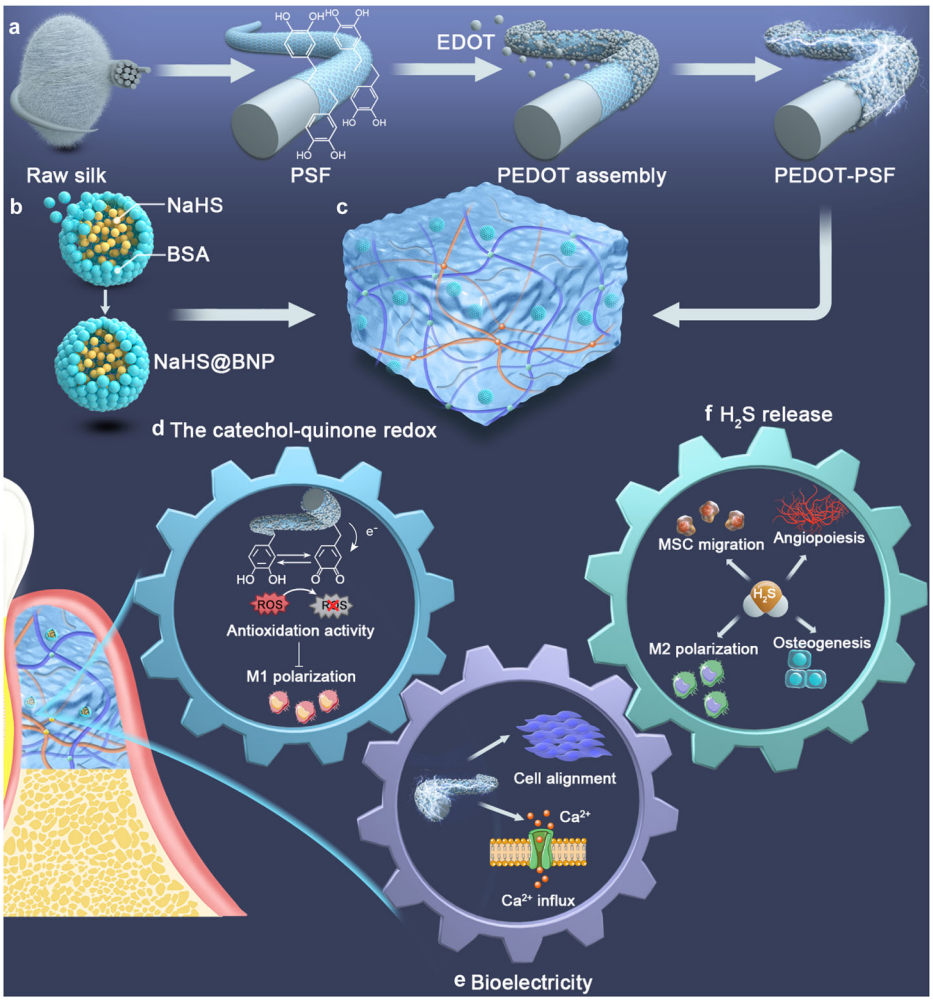

Fig. 1 | Schematic illustration of the synthesis and properties of the polyphenol-mediated redox-active hydrogel with H_2S gaseous-bioelectric coupling. **a** Schematic diagram of PEDOT-PSF synthesis. **b** Schematic diagram of BNPs synthesis. **c** The BNP-PEDOT-PSF hydrogel. **d** PDA endows the hydrogel with the ability of antioxidative and immunomodulatory. **e** The conductive hydrogel transmits endogenous bioelectricity and consequently improves cell alignment and increases Ca^{2+} influx. **f** H_2S released from BNPs promotes MSCs migration, angiopoiesis, osteogenesis, and M2 macrophage polarization. MSC mesenchymal stem cell.

Furthermore, to investigate the reduction of quinone groups into catechol groups by conductivity PEDOT-PSF and reductive H_2S, PSF, PEDOT-PSF, and H_2S treated PEDOT-PSF were examined using X-ray photoelectron spectroscopy (XPS). After assembly of conductive PEDOT on the surface of PSF, the content of C-O groups increased from 31.71 ± 8.28 to 57.60 ± 3.88%, and the content of C = O groups decreased from 68.29 ± 8.28 to 42.40 ± 3.88%, which implies that quinone groups were reduced to catechol groups through the electron transfer from PEDOT to PDA (Fig. 2f, g, Supplementary Table 3). Reductive H_2S further increased the content of C-O groups from 57.60 ± 3.88 to 64.39 ± 1.24% and deceased the content of C = O groups from 42.40 ± 3.88% to 35.61 ± 1.24%, protecting the phenol groups from oxidation (Fig. 2g, h, Supplementary Table 3). The results demonstrated that this system has redox activity. In addition, SEM images showed that AG hydrogel incorporating the BNPs and PEDOT-PSF (BNP-PEDOT-PSF-AG) had a uniform porous structure (Fig. 2i). BNPs and PEDOT-PSF were embedded in the hydrogel (Fig. 2i). Notably, PSF-AG hydrogel had denser and more uniform microstructures than the hydrogel without PSF (Supplementary Fig. 4a). Moreover, incorporation of BNPs did not change the microstructure of the hydrogel. After incorporation of BNPs, the hydrogel could sustain release of H_2S for 21 days (Fig. 2j).

The ability to withstand compression is important for a periodontal regenerative hydrogel, since it must bear masticatory force upon implantation. Owing to the ultralong length and uniform dispersion of PEDOT-PSF in the hydrogel, stress can be transferred along the PEDOT-PSF in the system. Thus, PSF and PEDOT-PSF confer the AG hydrogels with good mechanical properties. With the addition of PSF and PEDOT-PSF, the compressive strength of the BNP-PEDOT-PSF-AG hydrogels increased from about 82 to 100 kPa (Supplementary Fig. 4b). Moreover, the BNP-PEDOT-PSF-AG hydrogels recovered quickly upon withdrawal of compression force after 10 cycles, indicating excellent recovery properties of the hydrogel (Fig. 2k). In addition, the introduce of PSF and PEDOT-PSF delayed the degradation of the hydrogels, which provided a stable place for cells in the early stage of alveolar bone repair (Supplementary Fig. 4d).

PEDOT-PSF also endows the hydrogels with good electrical conductivity (Fig. 2l–o). With the increase of PEDOT-PSF content, the conductivity of the BNP-PEDOT-PSF-AG hydrogel increased (Fig. 2l). The conductivity reached 13.12 ± 1.66 S/m with 2 wt ‰ PEDOT-PSF in the hydrogel, which was selected for the subsequent experiments (Fig. 2l). In a BNP-PEDOT-PSF-AG hydrogel-connected circuit, a light-emitting diode (LED) was illuminated upon connection (Fig. 2m). Notably, the LED maintained lighting during the whole process of compression and release, indicating excellent dynamic conductivity of the hydrogel (Fig. 2n). Moreover, the conductivity of the hydrogel was stable during the deformation (Fig. 2o) and in vivo 14 days after implantation (Supplementary Fig. 5).

https://doi.org/10.1038/s41467-024-53290-6

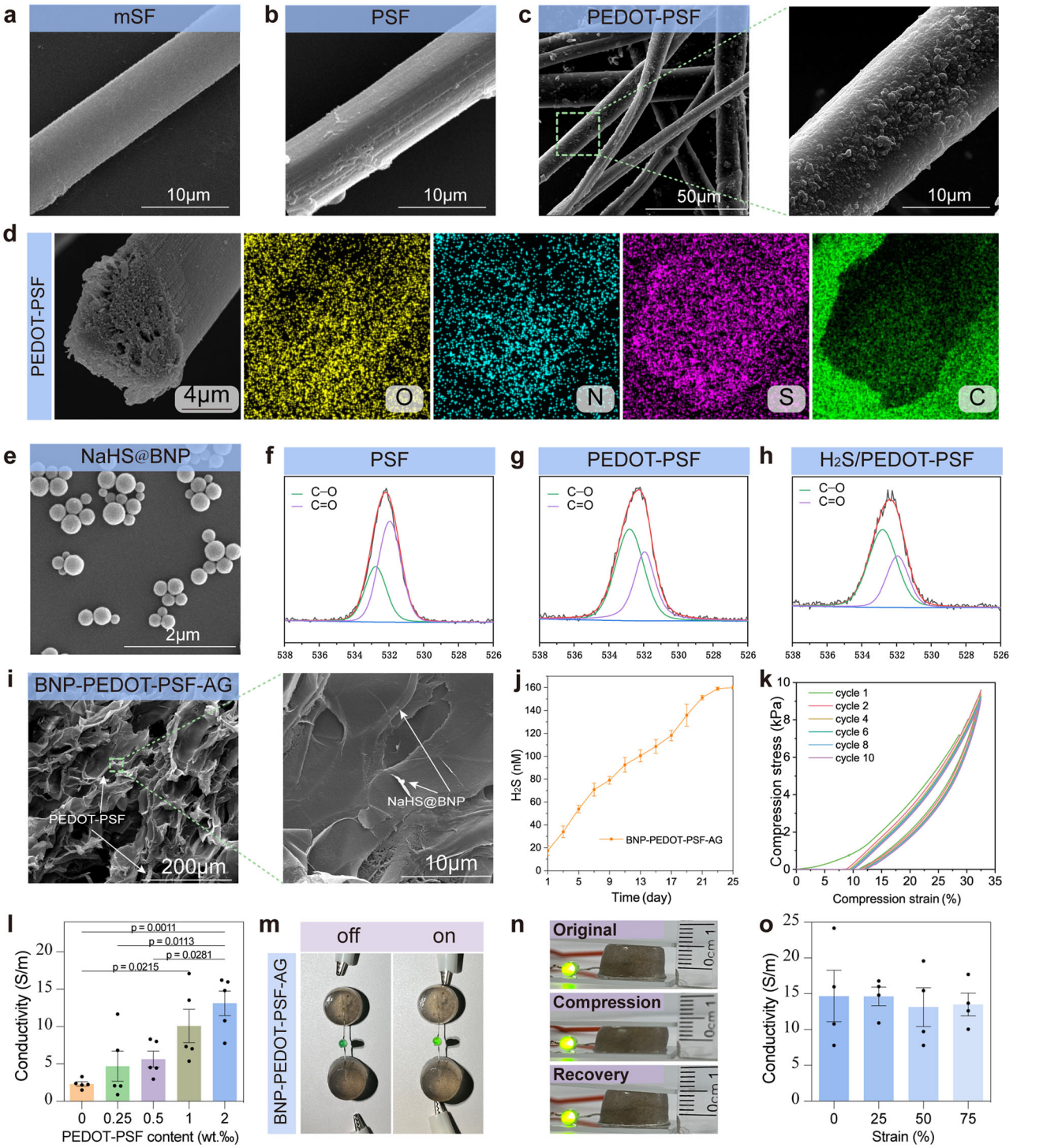

Fig. 2 | Characterization of the BNP-PEDOT-PSF hydrogel. SEM micrographs of mSF (**a**), PSF (**b**), and PEDOT-PSF (**c**). **d** Element mapping of PEDOT-PSF. **e** SEM micrograph of NaHS@BNP. XPS analysis of PSF (**f**), PEDOT-PSF (**g**), and H_2S treated PEDOT-PSF (**h**). **i** SEM micrographs of the BNP-PEDOT-PSF-AG hydrogel. Arrows indicate PEDOT-PSF and NaHS@BNP embedded in the hydrogel. **j** The amount of H_2S released from the BNP-PEDOT-PSF hydrogel in 25 days (mean ± SEM, $n = 4$ independent samples at each time point). **k** Cyclic compression test curve of the BNP-PEDOT-PSF-AG hydrogel. **l** Conductivities of hydrogels with different contents of PEDOT-PSF (mean ± SEM, $n = 5$ independent samples, one-way ANOVA). **m** A light-emitting diode (LED) was illuminated in a BNP-PEDOT-PSF-AG hydrogel-connected circuit. **n** The BNP-PEDOT-PSF-AG hydrogel with an illuminated LED was compressed and recovered. **o** Conductivity of the BNP-PEDOT-PSF-AG hydrogel after compression (mean ± SEM, $n = 4$ independent samples, one-way ANOVA).

Osteoinductive ability of the BNP-PEDOT-PSF-AG hydrogel in vitro

The BNP-PEDOT-PSF-AG hydrogel exhibited excellent potential to serve as a conductive platform for modulating cell proliferation, elongation, and osteogenesis under high-throughput electrical stimulation (ES). Human-derived periodontal ligament stem cells (PDLSCs) obtained from extracted premolars were cultured on the PEDOT-PSF-AG and BNP-PEDOT-PSF-AG hydrogel performed better in cell proliferation (Supplementary Fig. 6), demonstrating the proliferation of PDLSCs is not affected by the hydrogel. Moreover, as the

immunofluorescence staining images in Supplementary Fig. 7 show, PDLSCs on all of the hydrogels exhibited good ability to spread and adhere. Notably, cells on the PEDOT-PSF-AG hydrogel performed better in cell proliferation and elongation than those on hydrogels without conductivity. Specifically, the aspect ratio of the cells increased to 4.93 ± 0.45 at 600 mV from a baseline of 3.04 ± 0.16 without ES, indicating that ES improved the elongation of PDLSCs cultured on BNP-PEDOT-PSF-AG hydrogel (Supplementary Fig. 7b). According to previous research, the yield of osteogenesis increases with aspect ratio[42]. We also analyzed the expression of osteogenesis-related genes and ALP activity by the PDLSCs. Compared to the PSF-AG and AG groups, significantly higher expression of *OCN* (Fig. 3a) and *ALP* (Fig. 3b) and ALP activity (Fig. 3c) were found in the PEDOT-PSF-AG group under ES, confirming the osteoinductivity of PEDOT-PSF. Moreover, expression levels of *OCN* and *ALP*, and ALP activity in PDLSCs on BNP-PEDOT-PSF-AG hydrogel were significantly higher than on the PEDOT-PSF-AG hydrogels, indicating the osteogenic effects of H_2S. These results demonstrated that the conductive PEDOT-PSF and osteoinductive H_2S gas in the hydrogel synergistically improved osteogenic differentiation of PDLSCs. In addition, BNP-PEDOT-PSF-AG group showed the highest migration rate of PDLSCs, confirming the ability of H_2S in promoting PDLSC migration (Supplementary Fig. 8).

To explore the osteogenesis mechanism of PDLSCs on BNP-PEDOT-PSF-AG hydrogel, we performed transcriptome analyses of PDLSCs on PSF-AG, PEDOT-PSF-AG, and BNP-PEDOT-PSF-AG hydrogels after 3 days of culturing under high glucose and inflammatory conditions with 600 mV ES potentials. Pathway enrichment analysis of three groups include positive regulation of cell migration, angiogenesis, reactive oxygen species metabolic process, and positive regulation of osteoblast differentiation (Fig. 3d), which correlated with osteoinductive properties. Moreover, GSEA analysis showed downregulation of inflammation and upregulation of autophagy (Supplementary Fig. 9b). Based on existing evidence, upregulation of autophagy in PDLSCs promotes alveolar bone healing[43]. However, autophagy is impaired in periodontitis. Furthermore, the heatmap showed that *ATG2B*, *ATG12P1* were upregulated in the BNP-PEDOT-PSF-AG group. While *SQSTM1*, which negative regulates autophagy, was downregulated in the BNP-PEDOT-PSF-AG group, indicating augmentation of autophagy in BNP-PEDOT-PSF-AG group (Fig. 3e). Hence, we speculated that H_2S and bioelectricity promote osteogenesis through upregulation of autophagy.

Furthermore, enrichment analysis of 552 genes (excluded 90 genes shared by BNP-PEDOT-PSF-AG versus PSF-AG) between PEDOT-PSF-AG and PSF-AG, which representing the effect of bioelectricity included positive regulation of cell migration, cellular response to metal ion, cell adhesion, positive regulation of cell motility, regulation of actin cytoskeleton reorganization, cytokine-cytokine receptor interaction, and calcium signaling pathway, which correlated with the migration and adhesion of PDLSCs (Supplementary Fig. 9c). Interestingly, a growing body of scientific literature has revealed that ES induced Ca^{2+} influx plays a key role in osteogenic differentiation[44]. In this study, significantly upregulated intracellular Ca^{2+} were observed in PDLSCs on BNP-PEDOT-PSF-AG hydrogel under ES (Fig. 3f, g).

In summary, the osteoinductive ability of the hydrogels can be attributed to the following mechanisms (Fig. 3h). First, H_2S released from the BNPs and PEDOT-PSF synergistically promotes the osteogenic differentiation of the PDLSCs through augmentation of autophagy[43,45]. Second, PEDOT-PSF increases the intracellular Ca^{2+} derived from microenvironment and hydrogels, which promotes osteogenic differentiation[44]. Moreover, PEDOT-PSF enhances cell elongation, which also contributes to the enhanced osteogenic differentiation of the PDLSCs[42].

Antioxidative activities of the BNP-PEDOT-PSF-AG hydrogel in vitro

In this hydrogel, PDA plays an important role for scavenging the ROS via its catechol groups. However, during the process, the catechol groups were oxidized to the quinone groups, which would reduce its ROS-scavenging ability. Note that, mussel could remain its long-term adhesion in seawater through controlling the catechol-quinone redox balance. Inspired by mussel adhesion, we fabricated a PDA-mediated conductive silk fiber. The conductive fibers endow the hydrogel with good conductivity. Moreover, the electron could transfer from PEDOT to PDA, which cooperated with H_2S to facilitated the dynamic redox between catechol and quinone groups. In short, the PEDOT-PSF/H_2S provided a redox-activity for the hydrogel (Fig. 4a).

A 1,1-diphenyl-2-picrylhydrazyl (DPPH) free radical scavenging assay was employed to evaluate the antioxidative properties of the hydrogels. The results showed that the DPPH-scavenging ratios of PSF-AG, BNP-PSF-AG, PEDOT-PSF-AG, and BNP-PEDOT-PSF-AG hydrogels increased over time (Fig. 4b). The DPPH-scavenging ratio of PSF-AG hydrogel was higher than that of AG hydrogel owing to the antioxidative property of PDA on the surface of PSF. Notably, better antioxidative ability was observed in PEDOT-PSF-AG and BNP-PSF-AG hydrogel than PSF-AG hydrogel, due to enhancement of the catechol-quinone dynamic redox derived from the electron transfer from PEDOT to PDA or the release of H_2S from BNPs.

H_2S has been recognized as a reducing agent, as it regulates oxidative stress through direct reaction with ROS and reactive nitrogen species (RNS) and indirect effects on related enzymes or other targets in signaling pathways[46]. Specifically, hydrosulfide anions, dissociated from H_2S as powerful one electron chemical reductants, could transfer hydrogen atom or single electron at or near diffusion-controlled rates to quench free radicals[47]. Moreover, H_2S could attenuate cellular oxidative stress by improving the activities of related enzymes such as catalase and glutathione peroxidase (Gpx) or upregulating the levels of nonenzymatic antioxidants such as classic thioredoxin and reduced glutathione[48–50]. Owing to the synergetic effect of H_2S and PEDOT-PSF, the BNP-PEDOT-PSF-AG hydrogel achieved the highest DPPH-scavenging ratio among all tested hydrogels (Fig. 4b). This ROS-scavenging property endows the hydrogel with ability to protect cells from ROS damage.

Then, to measure the intracellular ROS levels in THP-1 cells cultured on different hydrogels, a 2′,7′-dichlorofluorescein diacetate (DCFH-DA) probe was applied. Similar to the tendency in the DPPH free radical scavenging assay, PSF-AG, BNP-PSF-AG, PEDOT-PSF-AG, and BNP-PEDOT-PSF-AG groups exhibited lower fluorescence intensity, representing lower ROS levels in cells (Fig. 4c, d). Among these four groups, the BNP-PEDOT-PSF-AG group showed the lowest fluorescence intensity, indicating excellent ROS-scavenging properties that we attribute to the synergistic effects of PEDOT-PSF and H_2S. Moreover, THP-1 cells cultured on the PEDOT-PSF-AG and BNP-PEDOT-PSF-AG hydrogels performed better in cell proliferation (Fig. 4e, f), demonstrating the proliferation of THP-1 is not affected by the hydrogels. Collectively, these results demonstrated that the BNP-PEDOT-PSF-AG hydrogel possesses excellent antioxidative ability.

Immunomodulatory activities of the BNP-PEDOT-PSF-AG hydrogel in vitro

The BNP-PEDOT-PSF-AG hydrogel also has immunomodulatory properties through shifting macrophage polarization from M1 to M2. The polarization of macrophages plays an important role in tissue regeneration. Specifically, M1 macrophages play a pro-inflammatory role and induce chronic inflammation, while M2 macrophages play an anti-inflammatory role and promote tissue remodeling[51]. However, M2 polarization is impacted under diabetic conditions[52]. To evaluate the immunomodulatory properties of the hydrogels, the number of

https://doi.org/10.1038/s41467-024-53290-6

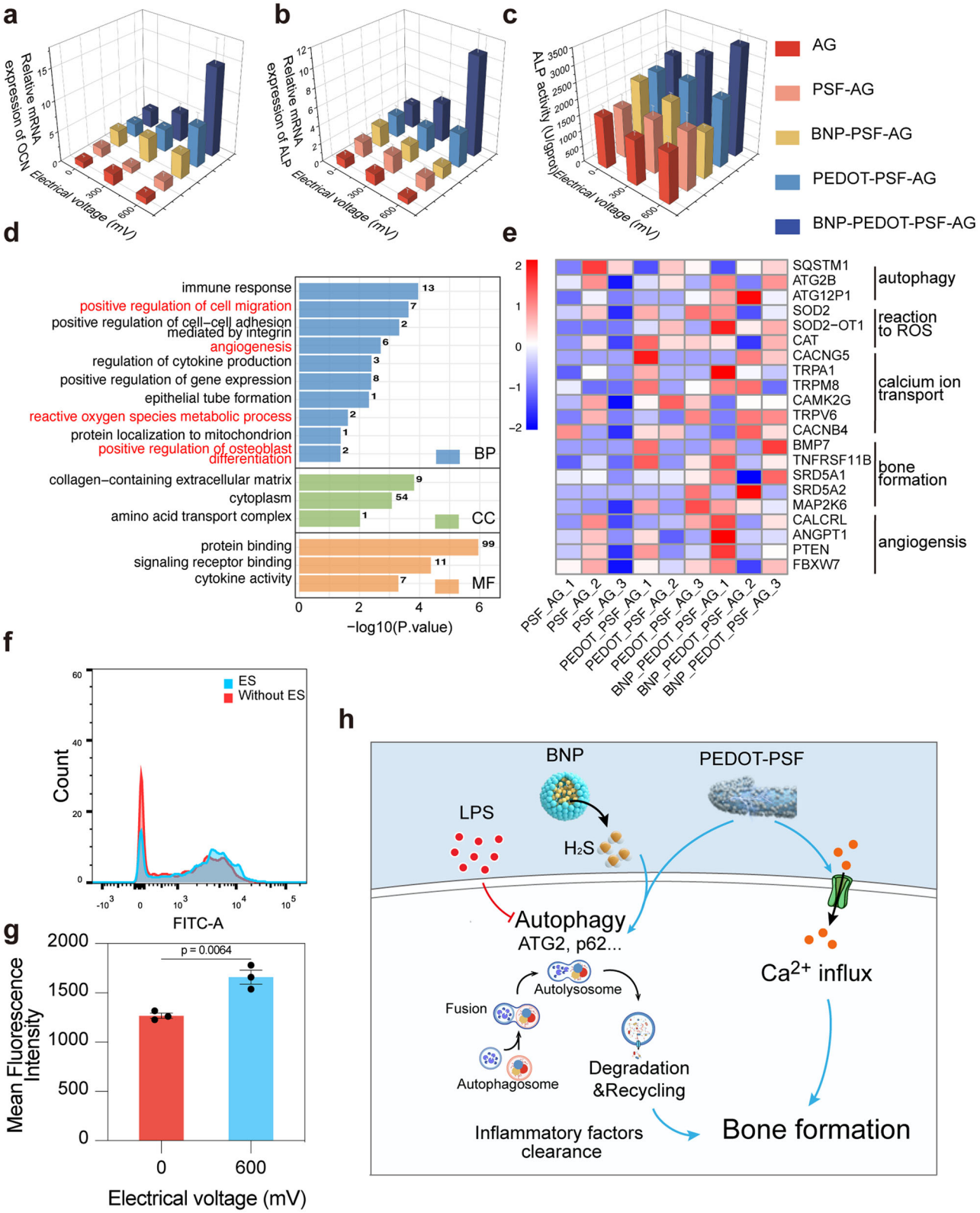

Fig. 3 | Osteogenesis of PDLSCs on the hydrogels under high throughput electrical stimulation (ES). Osteogenesis-related gene expressions of *OCN* (**a**) and *ALP* (**b**) in PDLSCs on the various hydrogels under various ES potentials ($n = 3$ independent biological samples).ES electrical stimulation. **c** ALP activity of PDLSCs on the various hydrogels under various ES potentials ($n = 3$ independent biological samples). **d** GO Enriched pathways of all genes in three groups. BP biological processes, CC cellular component, MF molecular functions. **e** Heatmap analysis of differentially expressed genes involved in autophagy, rection to ROS, calcium ion transport, bone formation and angiogenesis. ROS reactive oxygen species. **f** Flow cytometry of Fluo-8 AM-labeled cells in the fluorescein isothiocyanate (FITC)-A channel, indicating intracellular Ca^{2+} concentration of cells on the BNP-PEDOT-PSF-AG hydrogel with or without ES. **g** Quantification analysis for flow cytometric analysis of Ca^{2+} concentration in PDLSCs (mean ± SEM, $n = 3$ independent biological samples, two-tailed t-test). **h** Schematic illustration of the mechanism of osteoinductive ability of BNP-PEDOT-PSF-AG hydrogel on PDLSCs. The blue arrow showed the effect of the BNP-PEDOT-PSF-AG hydrogel. LPS lipopolysaccharides.

https://doi.org/10.1038/s41467-024-53290-6

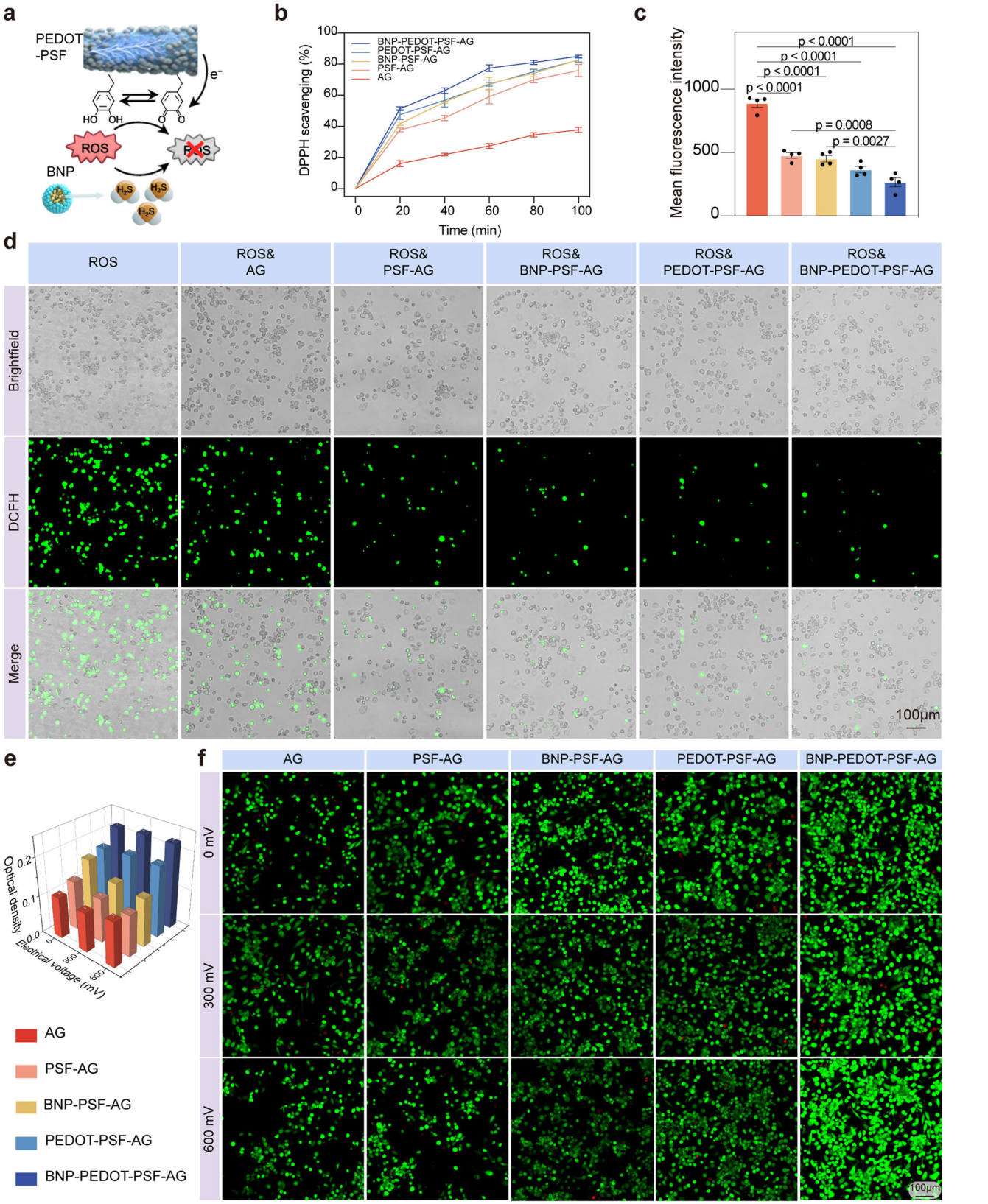

Fig. 4 | Antioxidative property of the BNP-PEDOT-PSF-AG hydrogel in vitro. **a** Antioxidative mechanism of the BNP-PEDOT-PSF-AG hydrogel. ROS, reactive oxygen species. **b** DPPH-scavenging efficiency of AG, PSF-AG, BNP-PSF-AG, PEDOT-PSF-AG, and BNP-PEDOT-PSF-AG hydrogels (mean ± SEM, $n = 3$ independent samples at each time point). **c** Quantification analysis for flow cytometric analysis of DCFH-DA-labeled cells in the FITC-A channel on the various hydrogels (mean ± SEM, $n = 4$ independent biological samples, one-way ANOVA). **d** Intracellular ROS-scavenging performance of THP-1 on the various hydrogels. **e** MTT analysis of THP-1 ($n = 4$ independent biological samples). **f** Live/dead staining of THP-1.

M1 macrophages and M2 macrophages were detected on various hydrogels. Compared to the AG group, the number of M1 macrophages in the PSF-AG, BNP-PSF-AG, PEDOT-PSF-AG, and BNP-PEDOT-PSF-AG groups significantly decreased, which indicated the ability of PSF to inhibit M1 macrophage polarization (Fig. 5a, b, Supplementary Fig. 10a, b). In addition, thanks to the excellent immunomodulation ability of H_2S, the BNP-PEDOT-PSF-AG group exhibited a significant increase in the number of M2 macrophages compared to the other groups. Moreover, the expression levels of macrophage polarization-related genes (*IL-1β*, *TNF-α*, *NOS2*, *DECTIN*, *IL-10*, and *ARG-1*) exhibited a similar trend (Supplementary Fig. 10c, d). Furthermore, expression of osteoclastogenic-related genes (*TRAP*, *NFATC1*, *CTSK*, and *C-FOS*) were detected in RAW 246.7 cells cultured on hydrogels for 3 days under high glucose and inflammatory conditions with the addition of receptor activator of nuclear factor kappa-B ligand (RANKL). Significantly decreased osteoclast activity in both the PEDOT-PSF-AG and BNP-PEDOT-PSF-AG groups indicated the excellent ability of PEDOT-PSF to inhibit osteoclastogenesis (Supplementary Fig. 11). In short, these results demonstrated that the BNP-PEDOT-PSF-AG hydrogel possesses excellent immunomodulatory and osteoclast-inhibiting activity.

To elucidate the immunomodulatory mechanism of the BNP-PEDOT-PSF-AG hydrogel, we performed transcriptome analyses of THP-1 cells on AG, PEDOT-PSF-AG, and BNP-PEDOT-PSF-AG hydrogels after 3 days of culturing under high glucose and lipopolysaccharides (LPS) stimulation. The enriched terms between three groups included the inflammatory response, innate immune response, and lipid metabolism related pathway (Supplementary Fig. 12). Further GSEA analysis showed that downregulation of lipid biosynthesis and regulation of lipid catabolism were presented in the BNP-PEDOT-PSF-AG group (Fig. 5c). Moreover, Gpx activity was also upregulated in the BNP-PEDOT-PSF-AG group (Fig. 5d). Based on existing evidence, lipid synthesis is important in the regulation of macrophage functions. Specifically, lipid biosynthesis is upregulated in M1 macrophages to regulate membrane remodeling and synthesis of inflammatory mediators[53,54]. While, lipid catabolism is upregulated in M2 macrophages to maintain oxidative phosphorylation (OXPHOS)[55]. In this study, the heatmap showed that lipid catabolic process and Gpx activity related genes, which prevented fatty acid (FA) accumulation in cells, were upregulated in the BNP-PEDOT-PSF-AG group. While, genes related to lipid biosynthesis process, which caused FA accumulation in BNP-PEDOT-PSF-AG group, were downregulated in the BNP-PEDOT-PSF-AG group (Fig. 5e). In addition, M1 related genes were downregulated in PEDOT-PSF-AG and BNP-PEDOT-PSF-AG groups (Fig. 5e). Notably, M2 related genes were upregulated in BNP-PEDOT-PSF-AG group, which was accordance with our in vitro results. Hence, we speculated that H_2S and bioelectricity modulate macrophage polarization through regulation of lipid metabolism (Fig. 5f).

Antioxidative and immunomodulatory activities of the BNP-PEDOT-PSF-AG hydrogel in vivo

To further explore the in vivo antioxidative and immunomodulatory activities of the hydrogels in the context of periodontitis, periodontitis rats with diabetes were generated through intraperitoneal injection of streptozotocin (STZ) and establishment of ligature-induced periodontitis for 4 weeks (Fig. 6a, Supplementary Fig. 13b). An incision was made in the gingiva on the mesial palatal side of the first molar, and hydrogel was implanted under the gingival flap (Supplementary Fig. 13c). Under diabetic conditions, oxidative stress is elevated, which exacerbates periodontal disease and negatively impacts periodontal regeneration[56]. Moreover, the undermined innate antioxidative defense system is unable to reverse the increase in oxidative stress[57]. Hence, eliminating excessive ROS production and correcting the imbalanced oxidative stress is crucial for treatment of diabetes-associated periodontal complications[58]. In order to investigate the antioxidative effect of hydrogels in periodontitis in diabetic environment, the extent of lipid peroxidation and the activity of antioxidative enzymes were detected. The level of oxidative stress was significantly increased in diabetic periodontitis compared to normal periodontium (Supplementary Fig. 13f and g). After hydrogel implantation, the ratio of GSH to GSSG, which represents the antioxidative ability, increased in all groups, revealing the therapeutic effect of scaling before hydrogel implantation (Fig. 6b). Specifically, the ratios of GSH to GSSG were higher in the PSF-AG, BNP-PSF-AG, PEDOT-PSF-AG, and BNP-PEDOT-PSF-AG groups compared to the blank and pure AG groups, demonstrating the antioxidative ability of PSF. The BNP-PEDOT-PSF-AG (2.82 ± 0.26) group exhibited highest GSH to GSSG ratio of all, indicating a synergistic effect of PEDOT-PSF and H_2S in alleviating oxidative stress. Furthermore, the examination of Gpx, a member of the innate antioxidant defense system, also showed the same trend. Notably, the level of Gpx was nearly twice as high in the BNP-PEDOT-PSF-AG group than in the AG group (Fig. 6c), indicating the excellent antioxidant effect of PEDOT-PSF and H_2S. Taken together, these results established that BNP-PEDOT-PSF-AG hydrogel facilitates the metabolism of excess oxidation products in the microenvironment of diabetic periodontitis, which can be attributed to the synergistic effects of PEDOT-PSF and H_2S. In addition, the hydrogels did not cause systemic toxicity (Supplementary Fig. 14).

To further explore the in vivo immunomodulatory activity of the hydrogels, the phenotypes of macrophages in periodontal tissue were detected after implantation of hydrogels. As shown in Fig. 6d, e and Supplementary Fig. 15a, the numbers of M1 macrophages in the PEDOT-PSF-AG ($4.88 \pm 0.76\%$), BNP-PSF-AG ($5.69 \pm 1.26\%$), and BNP-PEDOT-PSF-AG ($1.98 \pm 0.26\%$) groups were significantly decreased compared to the blank ($18.22 \pm 1.62\%$) and pure AG ($13.24 \pm 1.21\%$) groups, representing the ability of PSF to inhibit M1 macrophage polarization. In our analysis of M2 macrophages, there were no significant differences among the blank ($1.54 \pm 0.36\%$), AG ($2.40 \pm 0.54\%$), and PSF-AG ($2.47 \pm 0.28\%$) groups. Increased M2 macrophages were observed in the PEDOT-PSF-AG ($5.92 \pm 1.16\%$), BNP-PSF-AG ($6.56 \pm 0.67\%$), and BNP-PEDOT-PSF-AG ($8.76 \pm 0.90\%$) groups. Specifically, the BNP-PEDOT-PSF-AG group exhibit the highest proportion of M2 macrophages (Fig. 6e and Supplementary Fig. 15a). These trends were in accordance with the in vitro results, which verified the synergistic effects of PEDOT-PSF and H_2S on immunomodulatory activity.

In the process of bone remodeling, the balance between osteoblasts and osteoclasts maintains the functional structure of bone. Osteoclasts are active in the early stage of bone repair. However, due to the excessive inflammation in the diabetic environment, a high level of osteoclast activity remains, which negatively impacts functional bone repair[11,59]. Osteoclast activity in different groups was evaluated using TRAP staining (Fig. 6f). The numbers of $TRAP^+$ cells were obviously decreased in the BNP-PEDOT-PSF-AG, PEDOT-PSF-AG, BNP-PSF-AG, and PSF-AG groups compared to the blank and AG groups; the BNP-PEDOT-PSF-AG group had the lowest number, indicating synergistic effects of PEDOT-PSF and H_2S strongly inhibited osteoclast activity (Fig. 6f and Supplementary Fig. 15b).

The BNP-PEDOT-PSF-AG hydrogel promotes osteogenesis in diabetic periodontitis

PDLSCs possess multilineage differentiation potential and can differentiate into various tissues such as osteoid tissue, periodontal ligament-like connective tissue, and cementoid tissue, all of which play important roles in functional periodontal regeneration[60]. Therefore, we analyzed the number of PDLSCs ($CD90^+$ cells) in conjunction with six types of hydrogels to investigate the response of host stem cells to hydrogels during periodontium regeneration. At day 7, the numbers of $CD90^+$ cells in the BNP-PSF-AG, PEDOT-PSF-AG, and BNP-PEDOT-PSF-AG groups were significantly higher than in the blank and AG groups.

https://doi.org/10.1038/s41467-024-53290-6

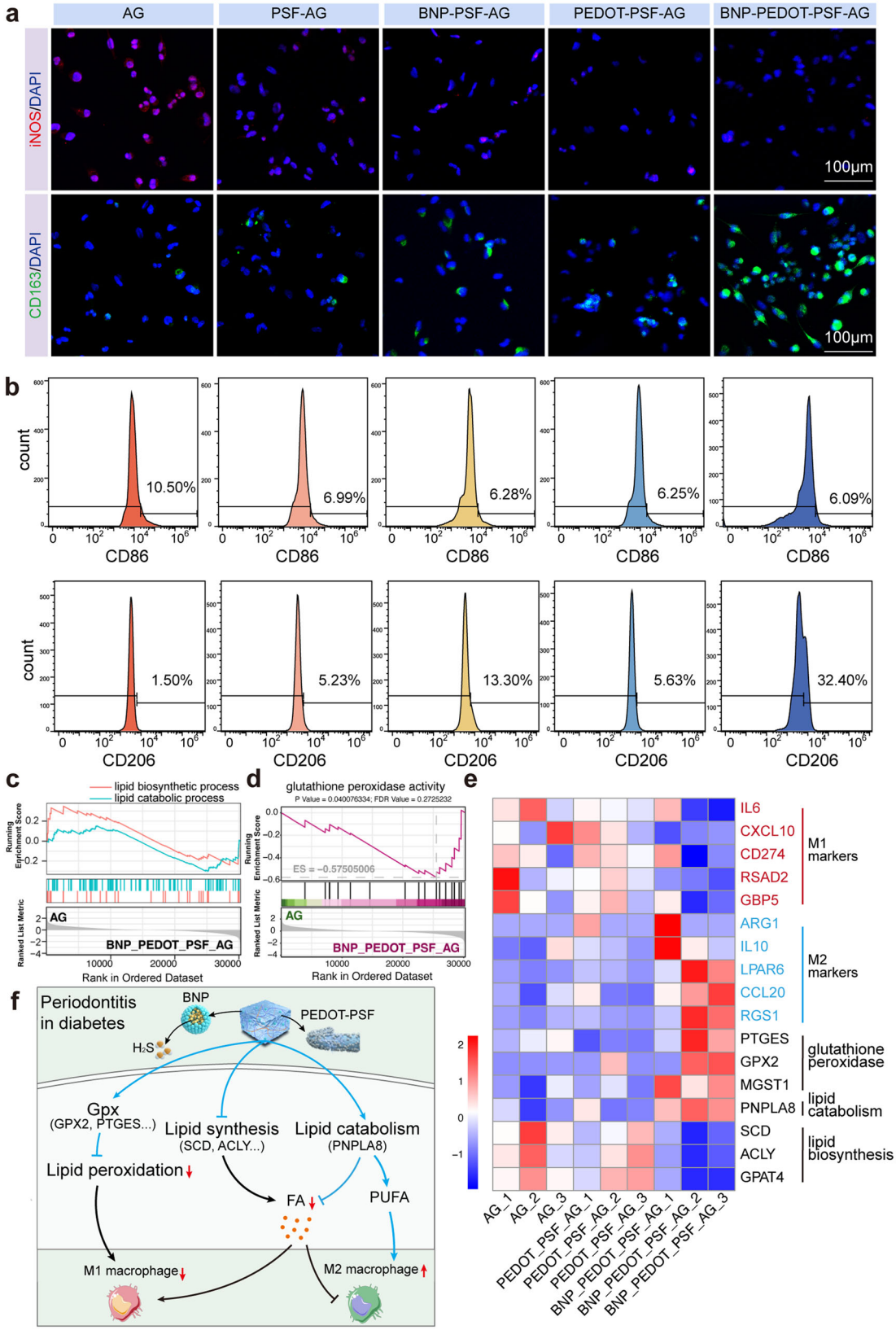

Fig. 5 | Immunomodulatory property and mechanism of the BNP-PEDOT-PSF-AG hydrogel in vitro. a Immunofluorescence staining of THP-1 cells on the different hydrogels. iNOS (red) stained M1 macrophages. CD163 (green) stained M2 macrophages. **b** Polarization of macrophages on the different hydrogels were evaluated by expression of CD86 (M1) and CD206 (M2) using flow cytometry. GSEA analysis of lipid catabolic process and lipid biosynthetic process (**c**) and glutathione peroxidase activity (**d**). **e** Heatmap of genes involved in macrophage polarization, lipid catabolic process, lipid biosynthetic process, and glutathione peroxidase activity. **f** Schematic illustration of the mechanism of immunomodulatory ability of BNP-PEDOT-PSF-AG hydrogel on THP-1. The blue arrow showed the effect of the BNP-PEDOT-PSF-AG hydrogel. Gpx glutathione peroxidase, FA fatty acid, PUFA polyunsaturated fatty acids.

https://doi.org/10.1038/s41467-024-53290-6

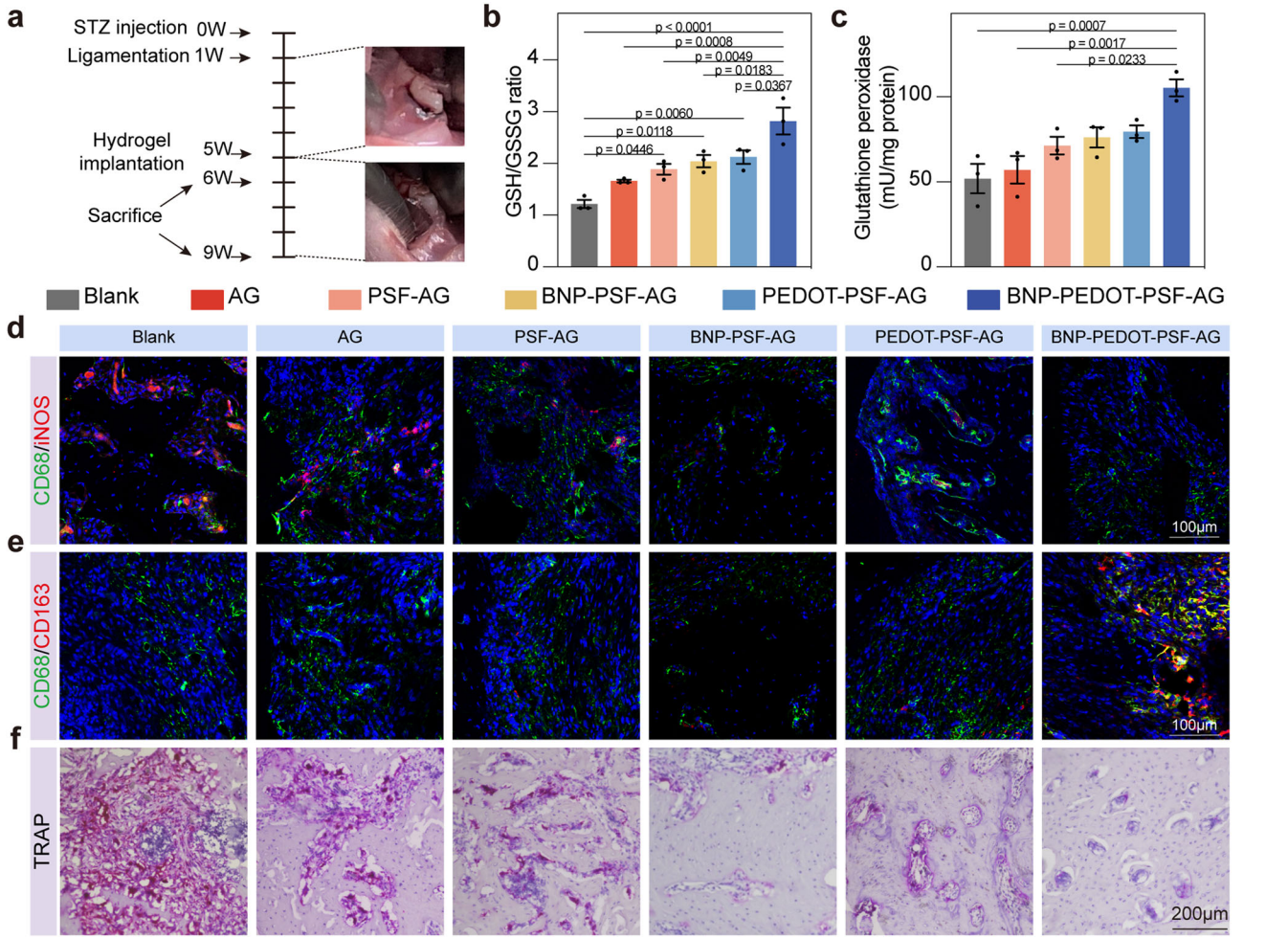

Fig. 6 | Antioxidative and immunomodulatory activities of the BNP-PEDOT-PSF-AG hydrogel in vivo. a The schedule of construction of periodontic rat with diabetes and hydrogel implantation. **b** GSH/GSSG ratio in defect area (mean ± SEM, $n = 3$ independent biological samples, one-way ANOVA). **c** Glutathione peroxidase level in defect area (mean ± SEM, $n = 3$ independent biological samples, one-way ANOVA). **d** Immunofluorescence staining of iNOS (red) and CD68 (green) double-stained M1 macrophages on the defect area. **e** Immunofluorescence staining of CD163 (red) and CD68 (green) double-stained M2 macrophages on the defect area. **f** TRAP staining of the defect area at 4 weeks after hydrogels implantation.

Notably, significantly more $CD90^+$ cells were observed in the BNP-PSF-AG (5.43 ± 0.46%) group compared to the PSF-AG group (2.83 ± 0.46 %) (Fig. 7a). Similarly, the number of CD90+ cells in the BNP-PEDOT-PSF-AG group (11.11 ± 0.97%) were significantly higher than that in the PEDOT-PSF-AG group (4.61 ± 0.53%), which was in accordance with the finding that the former group had the highest migration rate of PDLSCs in an in vitro wound scratch assay (Supplementary Fig. 8). These results indicated that H_2S is excellent at recruiting PDLSCs, which is essential in the early stage of periodontal regeneration.

It is well known that blood vessels and bone exhibit a close relationship in their spatial position as well as in their function. Cells, nutrients, oxygen, and growth factors needed for periodontal healing are transported to damaged periodontium through the blood[61]. Hence, angiogenesis is essential for periodontal regeneration. The ability of the hydrogels to promote revascularization was evaluated by the immunofluorescence of angiogenesis-related markers CD31 (Fig. 7b) and α-SMA (Fig. 7c) after 7 days of hydrogels implantation. The results showed that CD31 and α-SMA were highly expressed in the BNP-PEDOT-PSF-AG, PEDOT-PSF-AG, BNP -PSF-AG, and PSF-AG groups, representing positive effects of the anti-inflammatory microenvironment on revascularization. Moreover, the expression levels of CD31 in the BNP-PEDOT-PSF-AG group were significantly higher than in the other four groups without BNP, indicating that H_2S has excellent ability to promote angiogenesis (Fig. 6b). Furthermore, at 4 weeks post-surgery, the expression of osteogenesis-related factors (OCN and RUNX2) in the PEDOT-PSF-AG and BNP-PEDOT-PSF-AG groups were significantly higher than in the AG group, which is in accordance with the in vitro results, representing good osteoinductive ability of PEDOT-PSF (Fig. 7d, e). BNP-PSF-AG group also showed better higher expression of osteogenesis-related factors than AG group, indicating the ability of H_2S in bone formation (Fig. 7d, e). Specifically, the expression levels of OCN and RUNX2 in the BNP-PEDOT-PSF-AG group were highest among all five groups (Fig. 7d, e). These results indicated excellent revascularization and osteoinductive abilities of H_2S gas and PEDOT-PSF in the PSF-induced anti-inflammatory microenvironment.

The BNP-PEDOT-PSF-AG hydrogel promotes integrated periodontal regeneration in diabetic periodontitis

Micro-CT and histomorphological analysis were used to confirm the periodontal tissue repair promoted by the hydrogels at 4 weeks after surgical implantation of the hydrogels in the periodontitis rats with diabetes described above. The Micro-CT images showed that the ratio of bone volume to total volume in the BNP-PSF-AG (77.50 ± 1.56%), PEDOT-PSF-AG (84.25 ± 4.52%) and BNP-PEDOT-PSF-AG (90.35 ± 3.18%) groups was significantly increased compared to the

https://doi.org/10.1038/s41467-024-53290-6

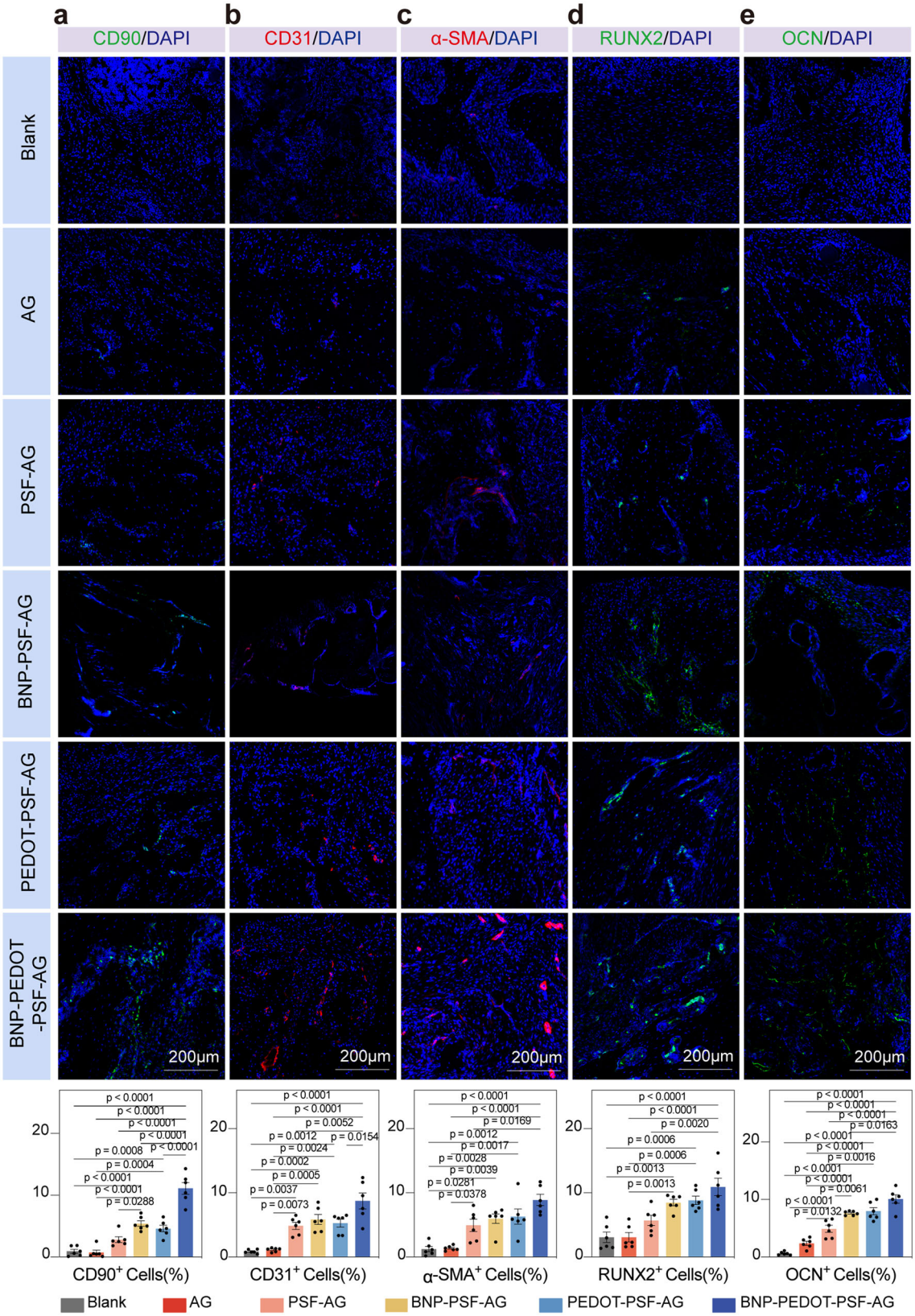

Fig. 7 | Immunofluorescence staining of defect areas. a Immunofluorescence staining of CD90 at 7 days after operation in defect area in various groups and quantification analysis (mean ± SEM, $n = 6$ independent biological samples, one-way ANOVA). Immunofluorescence staining of angiopoiesis-related protein CD31 (**b**) and α-SMA (**c**) at 7 days after operation in defect area and quantification analysis (mean ± SEM, $n = 6$ independent biological samples, one-way ANOVA). Immunofluorescence staining of osteogenesis-related protein RUNX2 (**d**) and OCN (**e**) at 4 weeks after operation in defect area and quantification analysis (mean ± SEM, $n = 6$ independent biological samples, one-way ANOVA).

https://doi.org/10.1038/s41467-024-53290-6

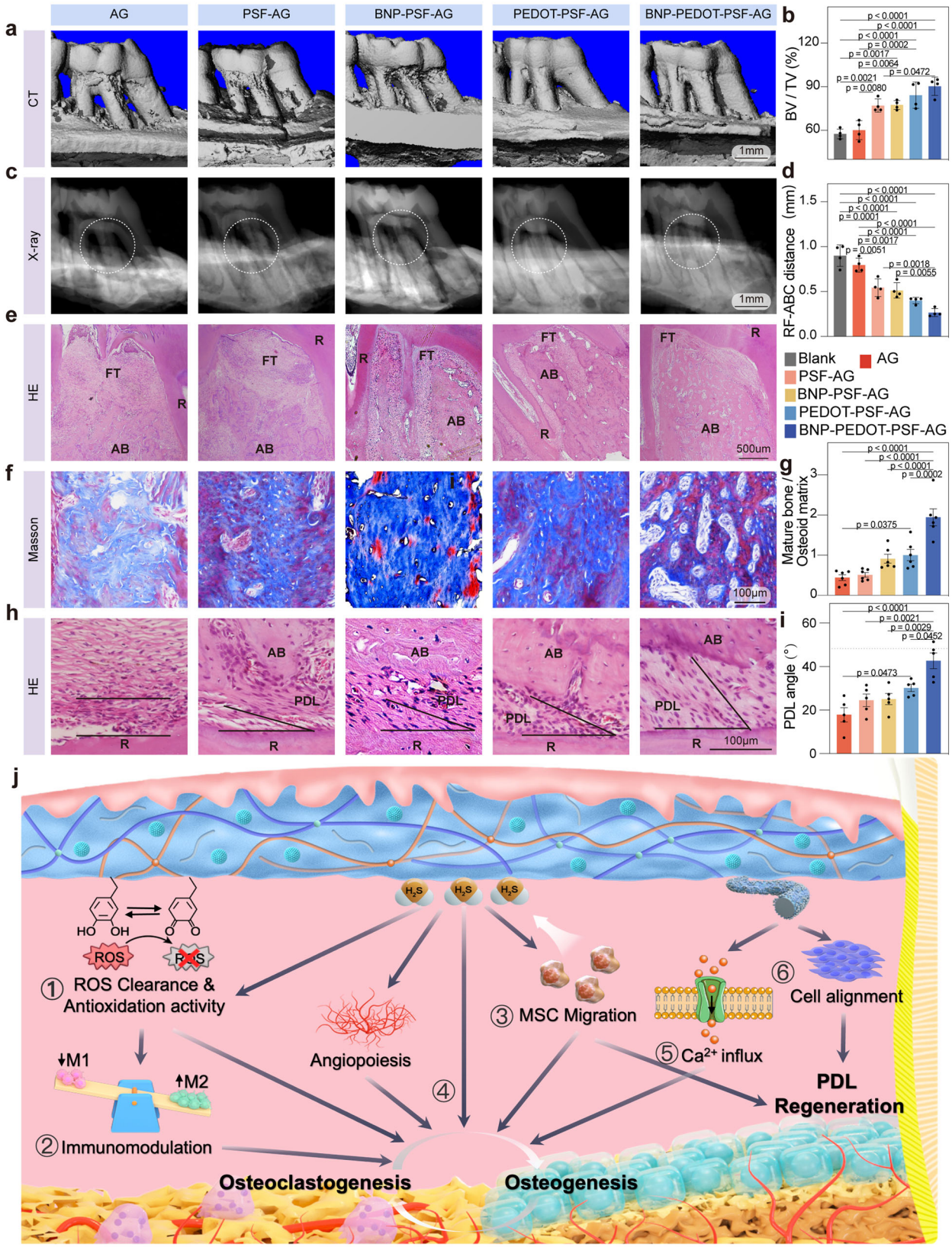

blank (57.54 ± 1.71 %) and AG (60.17 ± 3.28%) groups at 4 weeks post-surgery (Fig. 8a, b). Specifically, bone volume in BNP-PEDOT-PSF-AG was the highest among all six groups (Fig. 8a, b, Supplementary Fig. 13e). Furthermore, the distance between the root furcation and alveolar bone crest, which represents the amount of bone formation, in the six groups showed the same trend (Fig. 8c, d). These results confirmed the synergistic effects of PEDOT-PSF and H_2S in promoting bone regeneration in periodontitis under diabetic environment.

Histological analysis revealed that 4 weeks after hydrogel implantation, soft tissue occupied the space of alveolar bone loss under the root furcation in the AG and PSF-AG groups (Fig. 8e), whereas the BNP-PSF-AG, PEDOT-PSF-AG and BNP-PEDOT-PSF-AG

Fig. 8 | Periodontium regeneration in periodontitis under diabetic condition. **a**–**d** Micro-CT images of the rat maxillary first molar at the site of implantation. Quantification analysis of BV/TV (**b**) and RF-ABC distance (**d**) in the six groups (mean ± SEM, n = 4 independent biological samples, one-way ANOVA). BV bone volume, TV total volume, RF root furcation, ABC alveolar bone crest. **e** HE staining of the defect area at 4 weeks after implantation. AB alveolar bone. FT fiber tissue. R root. **f**, **g** Masson's trichrome staining of the defect area in various groups and quantification analysis (mean ± SEM, $n = 6$ independent biological samples, one-way ANOVA). **h** HE staining images of newly formed periodontal ligament. in periodontal defects at 4 weeks post-operation. The black angles indicated the angulation of newly formed periodontal ligament. PDL periodontal ligament. **i** Analysis of the angular values of newly formed ligaments for five groups, and dotted line represented average angle of native mature ligament fibers (mean ± SEM, $n = 5$ independent biological samples, one-way ANOVA). **j** Schematic illustration of the mechanism of the BNP-PEDOT-PSF-AG hydrogel in promoting integrate periodontium regeneration under diabetic periodontic condition. MSC mesenchymal stem cell, ROS reactive oxygen species, MSC mesenchymal stem cell.

groups exhibited more bone formation under the root furcation (Fig. 8e). Furthermore, the maturation of new bone was evaluated by Masson staining. The proportions of mature bone in both the PEDOT-PSF-AG (1.00 ± 0.14) and BNP-PEDOT-PSF-AG (1.94 ± 0.21) groups were significantly higher than in the AG (0.44 ± 0.07) group (Fig. 8f, g). Specifically, the maturation of new bone in the BNP-PEDOT-PSF-AG group was two times of that in the PEDOT-PSF-AG group. The superior alveolar bone formation in the BNP-PEDOT-PSF-AG group revealed the synergistic effects of H_2S and PEDOT-PSF on hard tissue regeneration in diabetic periodontitis.

The quality of periodontal fiber arrangement was reflected by the angles of periodontal ligament (PDL) fiber bundles relative to the root surface. Compared to the AG group (17.84 ± 3.31°), the PDL angles in the PEDOT-PSF-AG (30.20 ± 1.65°) and BNP-PEDOT-PSF-AG (42.65 ± 3.65°) groups were closer to the native mature angulation (48.21°)[62], which we attribute to the conductivity of PEDOT-PSF (Fig. 8h, i). Furthermore, the mean fiber angulation of the PDL in the BNP-PEDOT-PSF-AG group was higher than in the PEDOT-PSF-AG group (Fig. 8h, i). These findings demonstrated that PEDOT-PSF and H_2S not only promote bone formation, but also guide orderly arrangement of the PDL fibers, which is essential for functional PDL regeneration.

The excellent performance of the BNP-PEDOT-PSF-AG hydrogel in integrated periodontal regeneration in ta diabetic setting can be attributed to the following mechanisms (Fig. 8j): (1) Local inflammation and oxidative stress are alleviated by the hydrogels through excellent ROS-scavenging of PEDOT-PSF and H_2S. Subsequently, osteoclastogenesis is significantly reduced in the periodontal tissue. (2) The synergistic effect of PEDOT-PSF and H_2S modulates the local macrophage polarization through regulation of lipid metabolism. (3) MSCs are recruited to the periodontal tissue in a timely manner by the sustained release of H_2S from BNPs and then attach to the hydrogel thanks to the synergistic effect of PSF. Sufficient stem cells in the region ensure the subsequent angiogenesis. (4) Activated bone formation indued by synergetic effect of PEDOT-PSF and H_2S via promoting autophagy in PDLSCs. (5) PEDOT-PSF endows the hydrogel with good conductivity. The conductive hydrogels transmit endogenous bioelectricity and open Ca^{2+} ion channels under electric stimulation. The inflow of Ca^{2+} derived from AG hydrogels potentiate osteogenesis in situ. (6) The conductive hydrogels improve cell arrangement, enabling functional PDL regeneration. Together, these factors synergistically contribute to improving the periodontal environment and potentiating integrated periodontal regeneration under the conditions of diabetic periodontitis.

Discussion

In this study, the hydrogel was engineered by incorporating conductive PEDOT-PSF and a BNP-based H_2S sustained-release system into a physiochemical dual-crosslinked AG network. Compared with traditional biomaterials and biological modulation techniques, this study targeting the pathological microenvironment in diabetic periodontitis, creates a polyphenol-mediated redox-active hydrogel that couple endogenous bioelectricity and H_2S gas to reverse hyperglycemic inflammatory microenvironment. The hydrogel exhibits a number of advantages for periodontitis treatment in diabetes patients. First, the ultralong, uniformly dispersed PEDOT-PSF microfibers enhance the mechanical properties of the hydrogel, which meet the desired mechanical criteria for a periodontal local implant material. Second, PEDOT-PSF confers the hydrogel with excellent antioxidation and anti-inflammatory properties. With the synergistic effect of H_2S, the hydrogel exhibits immunomodulatory activity, which in turn converts inflammatory periodontium into a microenvironment favorable for regeneration. In addition, sustained release of H_2S from BNPs recruits MSCs to the periodontal tissue, promoting angiogenesis and osteogenesis. More importantly, with the PEDOT-PSF-facilitated conductive pathways, endogenous bioelectricity is transmitted to cells, which enhances Ca^{2+} influx and improves cell arrangement. Subsequently, the inflow of Ca^{2+} derived from the AG hydrogel potentiates osteogenesis in situ. Accordingly, the hydrogel achieves integrated periodontal bone healing through the synergistic effects of electrical conductivity, alleviation of oxidative stress, reduction of inflammation, immunomodulation, MSC recruitment, and osteogenesis. Therefore, this strategy for the coupling of H_2S gas and electrobiological activity could be a prospective strategy for the treatment of periodontitis in diabetes.

Methods

This study was approved by the Research Ethics Committee of West China Hospital of Stomatology (WCHSIRB-D-2021-163). The study design and conduct complied with the Department of Health and Human Services, the Declaration of Helsinki, and all relevant ethical regulations. Written, informed consent was provided by all patients before enrollment. All animal experiments were performed according to protocols approved by the Research Ethics Committee of West China Hospital of Stomatology (WCHSIRB-D-2020-485).

Fabrication of PEDOT-PSF

First, PSF was fabricated through a PDA-Assisted Protection-Extraction Process. Silk cocoons was boiled in a Na_2CO_3 solution (pH = 9) for 30 min, and stirred (room temperature) for 60 min. Then, the dried and degummed mSF (0.6 g) were immersed and stirred in dopamine (DA) tris-HCl buffer (0.05 M, 180 mL, pH = 8) for 10 h. Afterward, the solution was rested with half of the solution replaced to DI water. Subsequently, NaOH (0.42 g) was added in the solution (70 °C) for 3 h and sonicated for 1 h. Finally, the PSF was obtained after centrifugation for 3 times[63].

Then, PEDOT-PSF was prepared through Assisted PEDOT Assembly. PSF (0.05 g), EDOT (200 µL), and $FeCl_3{\cdot}6H_2O$ (1 g) were dispersed in 50 mL EtOH/H2O (3:1) solution. After 3 h, the PEDOT-PSF was obtained after centrifugation, washing, and drying[63].

Syntheses of NaHS@BNP

BNPs were fabricated by the desolvation method[64]. BSA (0.6 g) were added to distilled water (30 mL). NaHS (0.03 g) were dissolved in Ethanol (30 mL) to form the NaHS/Ethanol complex. Then the NaHS/Ethanol complex was added to BSA solution at rate of 0.5 mL/min. 18.75 mg N-(3-dimethylaminopropyl)- N′-ethylcarbodiimide hydrochloride (EDC) was added to the mixture for BNPs coupling. After stirring for 12 h, the NaHS-loaded BNPs were collected by centrifugation (19,760 × g, 15 min, 4 °C).

Preparation of the BNP-PEDOT-PSF-AG hydrogel

For synthesis of the BNP-PEDOT-PSF-AG hydrogel, 0.8 g of gelatin were dissolved in 10 ml 2 wt. % sodium alginate. The solution was stirred for 1 h at 65 °C until the gelatin powders were completely dissolved. 0.02 g PEDOT-PSF and 0.01 g BNPs were then added to the mixture, 600 µL PEGDE was added to the mixed solution to cross-link the gelatin. After 24 h cross-link, the hydrogel was soaked in 5% $CaCl_2$ solution for 1 h to further cross-link of the sodium alginate. For comparison, we prepared the PEDOT-PSF-AG hydrogels, BNP-PSF-AG hydrogels, PSF-AG hydrogels and AG hydrogels using the same assembly processes. The detailed contents are listed in Supplementary Table 1.

Characterizations of hydrogels

The morphology characteristics and structure of mSF, PSF, PEDOT-PSF, NaHS@BNP, and the BNP-PEDOT-PSF-AG hydrogel were observed by scanning electron microscopy (SEM, JSM 6390, JEOL). The H_2S release profiles were conducted by immersing the BNP-PEDOT-PSF-AG hydrogels in PBS at 37 °C. Then, H_2S releasing profile was measured by endogenous hydrogen sulfide (H_2S) assay kit (Catalog number: A146-1-1, Nanjing JianCheng Bioengineering Institute).

XPS analysis for recharging reduction of PSF, PEDOT-PSF, and H_2S/PEDOT-PSF

X-ray photoelectron spectroscopy (XPS; Kratos, Axis Ultra DLD, DK) was used to investigate the reduction of quinone groups into phenolic hydroxyl groups. PSF, PEDOT-PSF, and H_2S treated PEDOT-PSF were tested. The H_2S treated PEDOT-PSF were prepared by soaking PEDOT-PSF in NaHS solution for 30 min. A monochromatic Al Kα X-ray source (hν = 1486.6 eV) running at 15 kV and 150 W was used. Regarding the PSF, the O 1 s spectrum was fitted to 2 components: the hydroxyl group C-O at ~532.8 eV and the carbonyl group C = O at ~531.9 eV.

Mechanical property test

The compressive and tensile properties of hydrogel were measured by the universal testing machine (Instron 5567, Boston, MA, USA). The compressive strength, tensile strength strain at fracture were subsequently statistically analyzed. Tensile tests of the samples (width: 15 mm, length: 30 mm, thickness: 2 mm) were performed at an extension speed of 10 mm/min. The cyclic stress-strain test of BNP-PEDOT-PSF-AG hydrogels (10 mm (height) × 15 mm (diameter)) were performed at a speed of 5 mm/min; the maximum strain was 80%.

Conductivity measurement

The conductivities of the BNP-PEDOT-PSF-AG hydrogels (10 mm (height) × 15 mm (diameter)) were measured by a two-probe method using electrochemical system (CHI 660, Chenghua, China), according to our previous study[63]. The conductivity (κ, S/m) was calculated by $\kappa = \left(\frac{I}{V}\right)\left(\frac{L}{A}\right)$, where A and L are the cross-sectional area and height of the hydrogel, respectively. Conductivity of hydrogels with different contents of PEDOT-PSF and compression also exhibited by light-emitting diode (LED) test.

Cell culture

After administration of local anesthesia, the premolars were loosed and removed from its socket. 20 extracted premolars from 10 patients were obtained and immediately immersed in PBS containing 5% penicillin/streptomycin (Catalog number: P1400, Solarbio) at 4 °C. Then periodontal ligament was isolated from medium 1/3 of root[65]. After digested with collagenase I (Catalog number: 8140, Solarbio) at 37 °C for 1 h, tissues and cells were cultured with α-MEM medium containing 10% fetal bovine serum (Catalog number: 100–700, Gemini) and 1% penicillin/streptomycin. PDLSCs were used at passage 2–4. All tests performed under high glucose and inflammatory conditions (33 mM glucose,100 µg/L LPS).

Transcriptome sequencing and data analysis

PDLSCs were cultured with the BNP-PEDOT-PSF-AG, PEDOT-PSF-AG, and PSF-AG hydrogels under high glucose and inflammatory conditions (33 mM glucose,100 µg/L LPS) for 3 days with electrical stimulation (600mV). THP-1 cells were cultured with the BNP-PEDOT-PSF-AG, PEDOT-PSF-AG, and AG hydrogels under high glucose and inflammatory conditions (33 mM glucose,100 µg/L LPS) for 3 days. The PDLSCs and THP-1 cells were then treated with Trizol reagent (Invitrogen) and stored at −80 °C before sequencing. RNA sequencing was performed using Illumina HiSeq X10 (Illumina). Bioinformatic analysis was performed using the OmicStudio tools (https://www.omicstudio.cn/tool).

High-throughput electrical stimulation of PDLSCs

Different ES levels (0, 300 and 600 mV) were applied to PDLSCs on hydrogels for 30 min per day through a home-made high-throughput ES device[63,66]. After 3 days application of ES, cell proliferation and cell morphologies were measured. The cells were stained with cyanine dye 3 (Cy3)-conjugated phalloidin diluted in PBS with 1% BSA (F-actin; 1:500, Catalog number: 23111, ATT Bioquest). The cell spreading area of PDLSCs on the different hydrogels was analyzed using the ImageJ software. The cell viability was quantified using a 3-(4,5-dimethylthiazol-2-yl)-2,5-diphenyltetrazolium bromide (MTT) assay.

RNA extraction and quantitative real-time polymerase chain reaction (PCR)

After application of ES, total RNA was extracted from cell samples using RNA Extraction Kit (Tsingke). Then synthesized complementary DNA (cDNA) were gained using HiScript III RT SuperMix for RT-PCR (Vazyme). The primers used for target genes purchased from Tsingke are listed in Supplementary Table 2. All samples were performed in triplicate. The relative mRNA expression was normalized to GAPDH and calculated using the $2^{-\Delta\Delta Ct}$ method.

Intracellular calcium measurement

PDLSCs were seeded on the BNP-PEDOT-PSF-AG hydrogel and cultured at 37 °C for three days, followed by treatment with 30 min ES (600 mV) or without ES per day. Then cells were incubated with Fluo-8 AM (Catalog number: B21080, AAT Bioquest) for 30 min at 37 °C and collected for flow cytometry test (FACSAriaIII, BD).

Cellular ROS scavenging activity

A reactive oxygen species assay kit (2′,7′-dichloro fluorescein diacetate, DCFH-DA; Catalog number: S0033S, Beyotime) was used to test the cellular ROS scavenging activity. THP-1 cells were cultured with AG, PSF-AG, BNP-PSF-AG, PEDOT-PSF-AG, or BNP-PEDOT-PSF-AG hydrogels in 12-well plates for 12 h. After incubation with a DCFH-DA probe for 20 min, the ROS levels were measured using CLSM (NI-E, Nikon) and flow analyzer (FACSAriaIII, BD).

Polarization of macrophages

THP-1 cells were cultured with the BNP-PEDOT-PSF-AG, PEDOT-PSF-AG, BNP-PSF-AG, PSF-AG, and AG hydrogels under high glucose and inflammatory conditions (33 mM glucose,100 µg/L LPS) for 3 days. The cells were incubated with BV421 Mouse Anti-Human CD86 diluted in PBS (1:20; Catalog number: 562432; BD Biosciences) and FITC Mouse Anti-Human CD206 diluted in PBS (1:6; Catalog number: 551135; BD Biosciences) for 1 h at room temperature and analyzed using a flow analyzer (FACSAriaIII, BD, USA).

Establishment of diabetic periodontic rat model and hydrogel implantation

145 SD rats (male; 200–220 g; 8 weeks) were intraperitoneally injected with 55 mg/kg streptozocin (STZ; Sigma) to establish a diabetic model. In order to avoid experimental differences caused by sex, rats of the

same sex were used. After 1 week, the maxillary first molars of the rat were ligated with a 3-0 silk suture for 4 weeks to establish periodontitis. After palatal incision of the maxillary first molars and flap operation, AG, PSF-AG, BNP-PSF-AG, PEDOT-PSF-AG, or BNP-PEDOT-PSF-AG hydrogels (Φ 3 × 2 × 0.5 mm^3) were implanted into operation area to evaluate the osteoinductivity in vivo. Then the gingivae were sutured to fix the hydrogels. The rats were euthanized 7 and 28 days later. The samples were fixed for histology, immunofluorescence, and micro-CT assays.

Micro-computed tomography (μCT) and histology analysis of the periodontal repair

The harvested maxillaries were scanned with μCT (μCT50, SCANCO Medical) at 80 kV, 500 μA, and with a spatial resolution of 15 μm. The built-in software of the microCT imaging system was applied for the analysis of the volume of newly formed bone. After μCT analysis, the fixed maxillaries were assigned to histological analysis. The tissue sections were prepared into 4 μm thickness parallel to the long axis of the skull. Hematoxylin/eosin (HE) and Masson trichrome staining were conducted to show the periodontal regeneration situation. The quantified analysis of the bone formation in Masson stain was illustrated by the ratio of mature bone to the osteoid matrix by the ImageJ 1.48 v software. Additionally, tartrate-resistant acid phosphatase (TRAP) staining labeled activated osteoclasts.

For immunofluorescence staining, the fixed samples were incubated in 30% sucrose, embedded in Tissue-Tek, and then cut into 8-μm-thick sections parallel to the long axis of the skull. The slides were incubated overnight (4 °C) with the following primary antibodies diluted in universal antibody diluent (Catalog number: WB500D; NCM Biotech): rat anti-CD68 (1:100; Catalog number: Ab53444; Abcam), rabbit anti-iNOS (1:100; Catalog number: ab15323; Abcam), mouse anti-CD163 (1:100; Catalog number: sc-58965; Santa Cruz), rat anti-CD90 (1:100; Catalog number: ab3105; Abcam), rabbit anti-CD31(1:500; Catalog number: ab182981; Abcam), rabbit anti-α-SMA (1:100; Catalog number: ab5694; Abcam), mouse anti-RUNX2(1:100; Catalog number: sc-101145; Santa Cruz), and rabbit anti-OCN(1:100; Catalog number: DF12303 ; Affinity). After three washes with PBS, the sections were incubated with secondary antibodies of donkey anti-rat Alexa Fluor 488 (1:800; Catalog number: A21208; Thermo Fisher Scientific), donkey anti-rabbit Alexa Fluor 555(1:800; Catalog number: A31572; Thermo Fisher Scientific), goat anti-mouse Alexa Fluor 555 (1:800; Catalog number: A21423; Thermo Fisher Scientific), donkey anti-mouse Alexa Fluor 488 (1:800; Catalog number: A32766; Thermo Fisher Scientific), and donkey anti- rabbit Alexa Fluor 488 (1:800; Catalog number: A32790; Thermo Fisher Scientific) for 1 h at RT in dark. Cellular nuclei were labeled with DAPI (Beyotime, Shanghai, China). Images were examined with confocal (N-STORM & A1, NIKON).

Measurement of GSH/GSSG ratio and Gpx in periodontium tissue

Periodontal tissue was extracted from of maxillary first molars 4 weeks after hydrogel implantation. Each piece was further ground with sufficient liquid nitrogen. Then GSH/GSSG ratio and Gpx were measured by GSH and GSSG Assay Kit (Catalog number: S0053, Beyotime) and Total Glutathione Peroxidase Assay Kit with NADPH (Catalog number: S0058, Beyotime).

Statistics and reproducibility

The sample size in each experiment is indicated in the figure or corresponding figure legends. The SEM micrographs were repeated three times independently with similar results. Comparisons for two groups were conducted by a two-tailed Student's *t* test. Comparisons among groups were assessed by one-way analysis of variance (ANOVA) (for multiple groups) followed by the Tukey-Kramer test. The results were expressed as means ± SEM, $P < 0.05$ was considered statistically.

Reporting summary

Further information on research design is available in the Nature Portfolio Reporting Summary linked to this article.

Data availability

All data are available within the Article, Supplementary Information or Source Data file. The RNA-Sequence data have been deposited in the database at GSA-Human under accession number HRA007887 and HRA007950. Source data are provided with this paper.

References

1. Polak, D. & Shapira, L. An update on the evidence for pathogenic mechanisms that may link periodontitis and diabetes. *J. Clin. Periodontol.* **45**, 150–166 (2018).
2. Könönen, E., Gursoy, M. & Gursoy, U. K. Periodontitis: A Multifaceted Disease of Tooth-Supporting Tissues. *J. Clin. Med.* **8**, 1135 (2019).
3. Graves, D. T., Ding, Z. & Yang, Y. The impact of diabetes on periodontal diseases. *Periodontology.* **82**, 214–224 (2020).
4. Genco, R. J., Graziani, F. & Hasturk, H. Effects of periodontal disease on glycemic control, complications, and incidence of diabetes mellitus. *Periodontol. 2000.* **83**, 59–65 (2020).
5. Sanz, M. et al. Scientific evidence on the links between periodontal diseases and diabetes: Consensus report and guidelines of the joint workshop on periodontal diseases and diabetes by the International Diabetes Federation and the European Federation of Periodontology. *J. Clin. Periodontol.* **45**, 138–149 (2018).
6. Simpson, T. C. et al. Treatment of periodontitis for glycaemic control in people with diabetes mellitus. *Cochrane Database Syst. Rev.* **4**, Cd004714 (2022).
7. Pilipchuk, S. P. et al. Integration of 3D Printed and Micropatterned Polycaprolactone Scaffolds for Guidance of Oriented Collagenous Tissue Formation In Vivo. *Adv. Healthc. Mater.* **5**, 676–687 (2016).
8. Chen, F. M., Sun, H. H., Lu, H. & Yu, Q. Stem cell-delivery therapeutics for periodontal tissue regeneration. *Biomaterials* **33**, 6320–6344 (2012).
9. Cheng, G., Yin, C., Tu, H., Jiang, S. & Li, Z. Controlled Co-Delivery of Growth Factors through Layer-By-Layer Assembly of Core-Shell Nanofibers for Improving Bone Regeneration. *Acs. Nano.* **13**, 6372–6382 (2019).
10. Tan, J. et al. Sustained Release of Two Bioactive Factors from Supramolecular Hydrogel Promotes Periodontal Bone Regeneration. *Acs. Nano.* **13**, 5616–5622 (2019).
11. Wu, Y. Y., Xiao, E. & Graves, D. T. Diabetes mellitus related bone metabolism and periodontal disease. *Int. J. Oral. Sci.* **7**, 63–72 (2015).
12. Zhang, B., Yang, Y., Yi, J., Zhao, Z. & Ye, R. Hyperglycemia modulates M1/M2 macrophage polarization via reactive oxygen species overproduction in ligature-induced periodontitis. *J. Periodontal Res.* **56**, 991–1005 (2021).
13. T. Kocher, J. König, W. S. Borgnakke, C. Pink & P. Meisel Periodontal complications of hyperglycemia/diabetes mellitus: Epidemiologic complexity and clinical challenge. *Periodontology*. **78**, 59–97 (2018).
14. Woo, H. N., Cho, Y. J., Tarafder, S. & Lee, C. H. The recent advances in scaffolds for integrated periodontal regeneration. *Bioact. Mater.* **6**, 3328–3342 (2021).
15. Choi, W. et al. Occlusive membranes for guided regeneration of inflamed tissue defects. *Nat. Commun.* **14**, 7687 (2023).
16. Sun, Q. et al. Curved Nanofiber Network Induces Cellular Bridge Formation to Promote Stem Cell Mechanotransduction. *Adv. Sci. (Weinh.).* **10**, e2204479 (2023).
17. Levin, M. Bioelectric signaling: Reprogrammable circuits underlying embryogenesis, regeneration, and cancer. *Cell* **184**, 1971–1989 (2021).

18. Lundberg, J. O. & Weitzberg, E. Nitric oxide signaling in health and disease. *Cell* **185**, 2853–2878 (2022).
19. Duda, G. N. et al. The decisive early phase of bone regeneration. *Nat. Rev. Rheumatol.* **19**, 78–95 (2023).
20. Wallace, J. L. & Wang, R. Hydrogen sulfide-based therapeutics: exploiting a unique but ubiquitous gasotransmitter. *Nat. Rev. Drug Discov.* **14**, 329–345 (2015).
21. Herrera, B. S. et al. The H2S-releasing naproxen derivative, ATB-346, inhibits alveolar bone loss and inflammation in rats with ligature-induced periodontitis. *Med. Gas. Res.* **5**, 4 (2015).
22. Gugliandolo, E. et al. Anti-inflammatory effect of ATB-352, a H2S? releasing ketoprofen derivative, on lipopolysaccharide-induced periodontitis in rats. *Pharmacol. Res.* **132**, 220–231 (2017).
23. Zhou, X. et al. SM22α-lineage niche cells regulate intramembranous bone regeneration via PDGFRβ-triggered hydrogen sulfide production. *Cell Rep.* **39**, 110750 (2022).
24. Jain, S. K. et al. Low levels of hydrogen sulfide in the blood of diabetes patients and streptozotocin-treated rats causes vascular inflammation? *Antioxid. Redox Signal.* **12**, 1333–1337 (2010).
25. Dutta, M. et al. Evaluation of plasma H2S levels and H2S synthesis in streptozotocin induced Type-2 diabetes-an experimental study based on Swietenia macrophylla seeds. *Asian Pac. J. Trop. Biomed.* **4**, S483–S487 (2014).
26. Durante, W. Hydrogen Sulfide Therapy in Diabetes-Accelerated Atherosclerosis: A Whiff of Success. *Diabetes* **65**, 2832–2834 (2016).
27. Coletta, C. et al. Hydrogen sulfide and nitric oxide are mutually dependent in the regulation of angiogenesis and endothelium-dependent vasorelaxation. *Proc. Natl Acad. Sci. USA* **109**, 9161–9166 (2012).
28. Papapetropoulos, A. et al. Hydrogen sulfide is an endogenous stimulator of angiogenesis. *Proc. Natl Acad. Sci. USA* **106**, 21972–21977 (2009).
29. Qabazard, B., Masocha, W., Khajah, M. & Phillips, O. A. H(2)S donor GYY4137 ameliorates paclitaxel-induced neuropathic pain in mice. *Biomed. Pharmacother.* **127**, 110210 (2020).
30. Song, Z. L. et al. Progress and perspective on hydrogen sulfide donors and their biomedical applications. *Med. Res. Rev.* **42**, 1930–1977 (2022).
31. Li, T. & Zeng, K. Probing of Local Multifield Coupling Phenomena of Advanced Materials by Scanning Probe Microscopy Techniques. *Adv. Mater.* **30**, e1803064 (2018).
32. Zhao, M., Rolandi, M. & Isseroff, R. R. Bioelectric Signaling: Role of Bioelectricity in Directional Cell Migration in Wound Healing. *Cold Spring Harb. Perspect. Biol.* **14**, a041236 (2022).
33. Harris, M. P. Bioelectric signaling as a unique regulator of development and regeneration. *Development* **148**, 180794 (2021).
34. Fukui, H. et al. Bioelectric signaling and the control of cardiac cell identity in response to mechanical forces. *Science* **374**, 351–354 (2021).
35. Petsakou, A. & Perrimon, N. Bioelectric regulation of intestinal stem cells. *Trends Cell Biol.* **33**, 555–567 (2023).
36. Khare, D., Basu, B. & Dubey, A. K. Electrical stimulation and piezoelectric biomaterials for bone tissue engineering applications. *Biomaterials* **258**, 120280 (2020).
37. Luo, R. et al. Reshaping the Endogenous Electric Field to Boost Wound Repair via Electrogenerative Dressing. *Adv. Mater.* **35**, e2208395 (2023).
38. Sanchez-Casanova, S. et al. Local delivery of bone morphogenetic protein-2 from near infrared-responsive hydrogels for bone tissue regeneration. *Biomaterials* **241**, 119909 (2020).
39. Xu, X. et al. An injectable and thermosensitive hydrogel: Promoting periodontal regeneration by controlled-release of aspirin and erythropoietin. *Acta Biomater.* **86**, 235–246 (2019).
40. Jiao, D. et al. Bidirectional differentiation of BMSCs induced by a biomimetic procallus based on a gelatin-reduced graphene oxide reinforced hydrogel for rapid bone regeneration. *Bioact. Mater.* **6**, 2011–2028 (2021).
41. Alfieri, M. L., Weil, T., Ng, D. Y. W. & Ball, V. Polydopamine at biological interfaces. *Adv. Colloid Interface Sci.* **305**, 102689 (2022).
42. Yao, X., Peng, R. & Ding, J. Effects of aspect ratios of stem cells on lineage commitments with and without induction media. *Biomaterials* **34**, 930–939 (2013).
43. Yuan, W. et al. Agaricus blazei Murrill Polysaccharide Attenuates Periodontitis via H(2) S/NRF2 Axis-Boosted Appropriate Level of Autophagy in PDLCs. *Mol. Nutr. Food Res.* **67**, e2300112 (2023).
44. Ciobanu, F., Golzio, M., Kovacs, E. & Teissié, J. Control by Low Levels of Calcium of Mammalian Cell Membrane Electropermeabilization. *J. Membr. Biol.* **251**, 221–228 (2018).
45. Gambari, L., Grigolo, B. & Grassi, F. Hydrogen Sulfide in Bone Tissue Regeneration and Repair: State of the Art and New Perspectives. *Int. J. Mol. Sci.* **20**, 5231 (2019).
46. Zhu, Z., Lian, X. & Bhatia, M. Hydrogen Sulfide: A Gaseous Mediator and Its Key Role in Programmed Cell Death, Oxidative Stress, Inflammation and Pulmonary Disease. *Antioxidant.* **11**, 2162 (2022).
47. Predmore, B. L., Lefer, D. J. & Gojon, G. Hydrogen sulfide in biochemistry and medicine. *Antioxid. Redox Signal.* **17**, 119–140 (2012).
48. Wallace, J. L. et al. Anti-inflammatory and cytoprotective actions of hydrogen sulfide: translation to therapeutics. *Antioxid. Redox Signal.* **22**, 398–410 (2015).
49. Kumar, R. & Banerjee, R. Regulation of the redox metabolome and thiol proteome by hydrogen sulfide. *Crit. Rev. Biochem. Mol. Biol.* **56**, 221–235 (2021).
50. Corsello, T., Komaravelli, N. & Casola, A. Role of Hydrogen Sulfide in NRF2- and Sirtuin-Dependent Maintenance of Cellular Redox Balance. *Antioxidant* **7**, 129 (2018).
51. Okamoto, K. et al. Osteoimmunology: The Conceptual Framework Unifying the Immune and Skeletal Systems. *Physiol. Rev.* **97**, 1295–1349 (2017).
52. Louiselle, A. E., Niemiec, S. M., Zgheib, C. & Liechty, K. W. Macrophage polarization and diabetic wound healing. *Transl. Res.* **236**, 109–116 (2021).
53. Batista-Gonzalez, A., Vidal, R., Criollo, A. & Carreño, L. J. New Insights on the Role of Lipid Metabolism in the Metabolic Reprogramming of Macrophages. *Front. Immunol.* **10**, 2993 (2019).
54. Song, Z., Xiaoli, A. M. & Yang, F. Regulation and Metabolic Significance of De Novo Lipogenesis in Adipose Tissues. *Nutrients* **10**, 1383 (2018).
55. Odegaard, J. I. & Chawla, A. Alternative macrophage activation and metabolism. *Annu. Rev. Pathol.* **6**, 275–297 (2011).
56. Ko, K. I., Sculean, A. & Graves, D. T. Diabetic wound healing in soft and hard oral tissues. *Transl. Res.* **236**, 72–86 (2021).
57. Salek-Maghsoudi, A. et al. Recent advances in biosensor technology in assessment of early diabetes biomarkers. *Biosens. Bioelectron.* **99**, 122–135 (2018).
58. Sczepanik, F. S. C. et al. Periodontitis is an inflammatory disease of oxidative stress: We should treat it that way. *Periodontology.* **84**, 45–68 (2020).
59. Lecka-Czernik, B. Diabetes, bone and glucose-lowering agents: basic biology. *Diabetologia* **60**, 1163–1169 (2017).
60. Trubiani, O. et al. Periodontal Ligament Stem Cells: Current Knowledge and Future Perspectives. *Stem Cells Dev.* **28**, 995–1003 (2019).
61. Ding, T., Kang, W., Li, J., Yu, L. & Ge, S. An in situ tissue engineering scaffold with growth factors combining angiogenesis and osteoimmunomodulatory functions for advanced periodontal bone regeneration. *J. Nanobiotechnol.* **19**, 247 (2021).
62. Shang, L. et al. Dimethyloxallyl glycine/nanosilicates-loaded osteogenic/angiogenic difunctional fibrous structure for functional periodontal tissue regeneration. *Bioact. Mater.* **6**, 1175–1188 (2021).

63. Jia, Z. et al. Bioinspired conductive silk microfiber integrated bioelectronic for diagnosis and wound healing in diabetes. *Adv. Funct. Mater.* **31**, 2010461 (2021).
64. Wang, Z. et al. Mussel-inspired nano-building block assemblies for mimicking extracellular matrix microenvironments with multiple functions. *Biofabrication* **9**, 035005 (2017).
65. Fang, X. Y. et al. CXCL12/CXCR4 Mediates Orthodontic Root Resorption via Regulating the M1/M2 Ratio. *J. Dent. Res.* **101**, 569–579 (2022).
66. Li, Y. et al. Polydopamine-mediated graphene oxide and nanohydroxyapatite-incorporated conductive scaffold with an immunomodulatory ability accelerates periodontal bone regeneration in diabetes. *Bioact. Mater.* **18**, 213–227 (2022).

Acknowledgements

This work was supported by National Natural Science Foundation of China (82271019 and 82471024 to J.W, 82072073, 82472149 to J.L, 82072073 and 32471392 to C.X, and 32201075 to Z.J), Fundamental Research Funds for the Central Universities (2682023ZTPY056 and 2682024ZTPY003 to C.X), Sichuan Science and Technology Program (24ZDYF0099 to J.W), Sichuan Health Commission Medical Science and Technology Program (21ZD003 to J.W), Research and Develop Program, and West China Hospital of Stomatology Sichuan University (RD-03-202101 to J.W), and New Interdisciplinary Cultivation Fund of SWJTU (2682023JX005 and 2682022KJ041 to C.X). The authors wish to acknowledge the assistance on materials characterization received from Analytical & Testing Center of the Southwest Jiaotong University.

Author contributions

J.L. and C.M.X. supervised the project. X.Y.F., C.X.Y.Y., Z.R.J., and J.L. performed the experiments. X.L., J.L.G., J.X., Y.M.Z., and J.H.R. participated in performing experiments and discussing the results; J.L., C.M.X., X.Y.F. and J.W analyzed the data and wrote the paper. X.Y.F. and J.W. contributed equally to this work. All authors discussed the results and have given approval to the final version of the paper.

Competing interests

The authors declare no competing interests.

Additional information

Supplementary information The online version contains supplementary material available at https://doi.org/10.1038/s41467-024-53290-6.

Correspondence and requests for materials should be addressed to Chaoming Xie or Jin Liu.

Peer review information *Nature Communications* thanks Gaolin Liang and the other, anonymous, reviewer for their contribution to the peer review of this work. A peer review file is available.

Reprints and permissions information is available at http://www.nature.com/reprints

Publisher's note Springer Nature remains neutral with regard to jurisdictional claims in published maps and institutional affiliations.

[1]Lab of Aging Research and Department of Geriatrics, State Key Laboratory of Biotherapy and National Clinical Research Center for Geriatrics, West China Hospital, Sichuan University, Chengdu 610041, PR China. [2]State Key Laboratory of Oral Diseases & National Center for Stomatology & National Clinical Research Center for Oral Diseases & Department of Orthodontics, West China Hospital of Stomatology, Sichuan University, Chengdu 610041, PR China. [3]Institute of Biomedical Engineering, College of Medicine, Southwest Jiaotong University, Chengdu 610031, PR China. [4]Hospital of Stomatology, Key Laboratory of Oral Biomedical Research of Zhejiang Province, School of Stomatology, Zhejiang University School of Medicine, Hangzhou 310016, PR China. [5]The Tenth Affiliated Hospital of Southern Medical University, Dongguan 523059, PR China. [6]These authors contributed equally: Xinyi Fang, Jun Wang ✉e-mail: xie@swjtu.edu.cn; liujin@scu.edu.cn